



1 **Evaluation of bacterial glycerol dialkyl glycerol tetraether and ^2H -**
2 **^{18}O biomarker proxies along a Central European topsoil transect**

3 Johannes Hepp^{1,2,*}, Imke K. Schäfer³, Verena Lanny⁴, Jörg Franke³, Marcel
4 Bliedtner^{3,a}, Kazimierz Rozanski⁵, Bruno Glaser², Michael Zech^{2,6}, Timothy I.
5 Eglinton⁴, Roland Zech^{3,a}

6 ¹Chair of Geomorphology and BayCEER, University of Bayreuth, 95440 Bayreuth, Germany and

7 ²Institute of Agronomy and Nutritional Sciences, Soil Biogeochemistry, Martin-Luther-University
8 Halle-Wittenberg, 06120 Halle, Germany

9 ³Institute of Geography and Oeschger Centre for Climate Change Research, University of Bern, 3012
10 Bern, Switzerland

11 ⁴Department of Earth Science, ETH Zurich, 8092 Zurich, Switzerland

12 ⁵Faculty of Physics and Applied Computer Science, AGH University of Science and Technology, 30-
13 059 Kraków, Poland

14 ⁶Institute of Geography, Faculty of Environmental Sciences, Technical University of Dresden, 01062
15 Dresden, Germany

16 ^anow at Institute of Geography, Chair of Physical Geography, Friedrich-Schiller University of Jena,
17 07743 Jena, Germany

18

19 *corresponding author (johannes-hepp@gmx.de)



20 **Keywords**

21 Leaf wax *n*-alkanes, hemicellulose sugars, pH, temperature, CBT, MBT[?], precipitation
22 $\delta^2\text{H}/\delta^{18}\text{O}$, relative humidity

23 **Abstract**

24 Molecular fossils, like bacterial branched glycerol dialkyl glycerol tetraethers (brGDGTs), and
25 the stable isotopic composition of biomarkers, such as $\delta^2\text{H}$ of leaf wax-derived *n*-alkanes ($\delta^2\text{H}_{n\text{-alkane}}$)
26 or $\delta^{18}\text{O}$ of hemicellulose-derived sugars ($\delta^{18}\text{O}_{\text{sugar}}$) are increasingly used for the
27 reconstruction of past climate and environmental conditions. Plant-derived $\delta^2\text{H}_{n\text{-alkane}}$ and
28 $\delta^{18}\text{O}_{\text{sugar}}$ values record the isotopic composition of plant source water ($\delta^2\text{H}/\delta^{18}\text{O}_{\text{source-water}}$),
29 which usually reflects mean annual precipitation ($\delta^2\text{H}/\delta^{18}\text{O}_{\text{precipitation}}$), modulated by
30 evapotranspirative leaf water enrichment and biosynthetic fractionation. Accuracy and
31 precision of respective proxies should be ideally evaluated at a regional scale. For this study,
32 we analysed topsoils below coniferous and deciduous forests, as well as grassland soils along a
33 Central European transect in order to investigate the variability and robustness of various
34 proxies, and to identify effects related to vegetation. Soil pH-values derived from brGDGTs
35 correlate reasonably well with measured soil pH-values, but systematically overestimate them
36 ($\Delta\text{pH} = 0.6 \pm 0.6$). The branched vs. isoprenoid tetraether index (BIT) can give some indication
37 whether the pH reconstruction is reliable. Temperatures derived from brGDGTs overestimate
38 mean annual air temperatures slightly ($\Delta T_{\text{MA}} = 0.5^\circ\text{C} \pm 2.4$). Apparent isotopic fractionation ($\epsilon_{n\text{-alkane/precipitation}}$
39 and $\epsilon_{\text{sugar/precipitation}}$) is lower for grassland sites than for forest sites due to “signal
40 damping”, i.e. grass biomarkers do not record the full evapotranspirative leaf water enrichment.
41 Coupling $\delta^2\text{H}_{n\text{-alkane}}$ with $\delta^{18}\text{O}_{\text{sugar}}$ allows to reconstruct the stable isotopic composition of the
42 source water more accurately than without the coupled approach ($\Delta\delta^2\text{H} = \sim 21\text{‰} \pm 22$ and
43 $\Delta\delta^{18}\text{O} = \sim 2.9\text{‰} \pm 2.8$). Similarly, relative humidity during daytime and vegetation period
44 (RH_{MDV}) can be reconstructed using the coupled isotope approach ($\Delta\text{RH}_{\text{MDV}} = \sim 17 \pm 12$).
45 Especially for coniferous sites, reconstructed RH_{MDV} values as well as source water isotope
46 composition underestimate the measured values. This can be likely explained by understory
47 grass vegetation at the coniferous sites contributing significantly to the *n*-alkane pool but only
48 marginally to the sugar pool in the topsoil. The large uncertainty likely reflect the fact that
49 biosynthetic fractionation is not constant, as well as microclimate variability. Overall, GDGTs
50 and the coupled $\delta^2\text{H}_{n\text{-alkane}}\text{-}\delta^{18}\text{O}_{\text{sugar}}$ approach have great potential for more quantitative
51 paleoclimate reconstructions.



52 **1 Introduction**

53 Information about the variability and consequences of past climate changes is a prerequisite for
54 precise predictions regarding the present climate change. Molecular fossils, so called
55 biomarkers, climate proxies have great potential to enhance our understanding about variations
56 of past climate and environmental changes. Lipid biomarkers in particular, are increasingly
57 used for paleoclimate and environmental reconstructions (e.g. Brincat et al., 2000; Eglinton and
58 Eglinton, 2008; Rach et al., 2014; Romero-Viana et al., 2012; Schreuder et al., 2016). However
59 strengths and limitations of respective proxies need known (Dang et al., 2016). For this,
60 calibrations using modern reference samples are essential.

61 Terrestrial branched glycerol dialkyl glycerol tetraethers (brGDGTs) that are synthesized in the
62 cell membranes of anaerobe heterotrophic soil bacteria (Oppermann et al., 2010; Weijers et al.,
63 2010) have great potential for the reconstruction of past environmental conditions (e.g. Coffinet
64 et al., 2017; Schreuder et al., 2016; Zech et al., 2012), although some uncertainties exist.
65 Calibration studies suggest that the relative abundance of the individual brGDGTs varies with
66 mean annual air temperature (T_{MA}) and soil pH (Peterse et al., 2012; Weijers et al., 2007), at
67 least across large, global climate gradients or along pronounced altitudinal gradients (Wang et
68 al., 2017). However, in arid regions the production of brGDGT is limited, while isoprenoidal
69 GDGTs (iGDGTs) produced by archaea provide the dominant part of the overall soil GDGT
70 pool (Anderson et al., 2014; Dang et al., 2016; Dirghangi et al., 2013; Wang et al., 2013; Xie
71 et al., 2012). The ratio of brGDGTs vs. isoprenoid GDGTs (BIT) can be used as indication
72 whether a reconstruction of T_{MA} and pH will be reliable. Moreover, Mueller-Niggemann et al.
73 (2016) revealed an influence of the vegetation cover on the brGDGT producing soil microbes.
74 From field experiments, it is known, that vegetation type and mulching practice strongly effect
75 soil temperature and moisture (Awe et al., 2015; Liu et al., 2014). Thus, multiple factors can be
76 expected to influence soil microbial communities and GDGT production. So far, little is known
77 about the variability of GDGT proxies on a regional scale, and a calibration study with small
78 climate gradient but with different vegetation types might be useful.

79 Compound specific stable hydrogen isotopes of leaf wax biomarkers, such as long chain n -
80 alkanes ($\delta^2H_{n\text{-alkanes}}$) record the isotopic signal of precipitation and therefore past climate and
81 environmental conditions (Sachse et al., 2004, 2006). However, various influencing factors are
82 known all along the way from the moisture source to leaf waxes (Pedentchouk and Zhou, 2018
83 and Sachse et al., 2012 for review). One is the evapotranspiration of leaf water (Feakins and
84 Sessions, 2010; Kahmen et al., 2013; Zech et al., 2015), which is strongly driven by relative air
85 humidity (RH; e.g. Cernusak et al., 2016 for review). In addition, a strong precipitation signal
86 is known to be incorporated into long chain leaf waxes (Hou et al., 2008; Rao et al., 2009;
87 Sachse et al., 2004). In paleoclimate studies, it is often not feasible to disentangle between the
88 evapotranspirative enrichment from the precipitation signal. Zech et al. (2013) proposed to
89 couple $\delta^2H_{n\text{-alkane}}$ results with oxygen stable isotopes of hemicellulose-derived sugars ($\delta^{18}O_{\text{sugar}}$).
90 Assuming constant biosynthetic fractionation factors (ϵ_{bio}) for the different compound classes
91 (n -alkanes and hemicellulose sugars), the coupling enables the reconstruction of the isotopic
92 composition of leaf water, RH and $\delta^2H/\delta^{18}O$ of plant source water ($\approx \delta^2H/\delta^{18}O$ of precipitation;
93 Tuthorn et al., 2015). So far, a detailed evaluation of this approach on the European scale, as
94 well as concerning possible effects related to vegetation changes is missing.



95 We analysed topsoil samples under coniferous, deciduous and grassland vegetation along a
96 Central European transect in order to estimate the variability of the biomarker proxies. More
97 specifically, we aim to test whether:

98 (i) the vegetation type has an influence on the brGDGT proxies, the $\delta^2\text{H}_{n\text{-alkane}}$ and the $\delta^{18}\text{O}_{\text{sugar}}$
99 stable isotopic composition, as well as on reconstructed $\delta^2\text{H}/\delta^{18}\text{O}_{\text{source-water}}$ and RH.

100 (ii) the published brGDGT proxies used for reconstructing mean annual temperature and soil
101 pH are sensitive enough to reflect the medium changes in temperature and soil pH along our
102 transect.

103 (iii) the coupled $\delta^2\text{H}_{n\text{-alkane}}-\delta^{18}\text{O}_{\text{sugar}}$ approach faithfully reflects $\delta^2\text{H}/\delta^{18}\text{O}$ of precipitation and
104 RH along the transect.

105

106 **2 Material and methods**

107 **2.1 Geographical setting and sampling**

108 In November 2012, we collected topsoil samples (0-5 cm depth) at 16 locations along a transect
109 from Southern Germany to Southern Sweden (Fig. 1A) and distinguished between sites with
110 coniferous forest (con, $n = 9$), deciduous forest (dec, $n = 14$) and grassland (grass, $n = 6$)
111 vegetation cover (for more details see Schäfer et al. (2016) and Tab. S1).

112

113 **2.2 Database of instrumental climate variables and isotope composition of precipitation**

114 Climate data was derived from close-by weather observation stations operating by the regional
115 institutions (Deutscher Wetterdienst (DWD) for Germany, Danmarks Meteorologiske Institut
116 (DMI) for Denmark and the Sveriges Meteorologiska och Hydrologiska Institute (SMHI) for
117 Sweden). The DWD provides hourly data for each station (DWD Climate Data Center, 2018b),
118 enabling not only the calculation of T_{MA} , but also of the mean annual relative air humidity
119 (RH_{MA}), mean temperature and relative air humidity during the vegetation period (T/RH_{MV}),
120 and of daytime temperature and relative humidity averages over the vegetation period
121 (T/RH_{MDV}). In addition, annual precipitation observations were used to derive the mean annual
122 precipitation amount (P_{MA} ; DWD Climate Data Center, 2018b). From the DMI, the respective
123 climate variables were derived from published technical reports (Cappelen, 2002; Frich et al.,
124 1997; Laursen et al., 1999). The SMHI provides open data from which we derived the climate
125 variables for the Swedish sites (Swedish Meteorological and Hydrological Institute, 2018). For
126 more details about the climate database used for calculations and comparisons, the reader is
127 referred to Tab. S2.

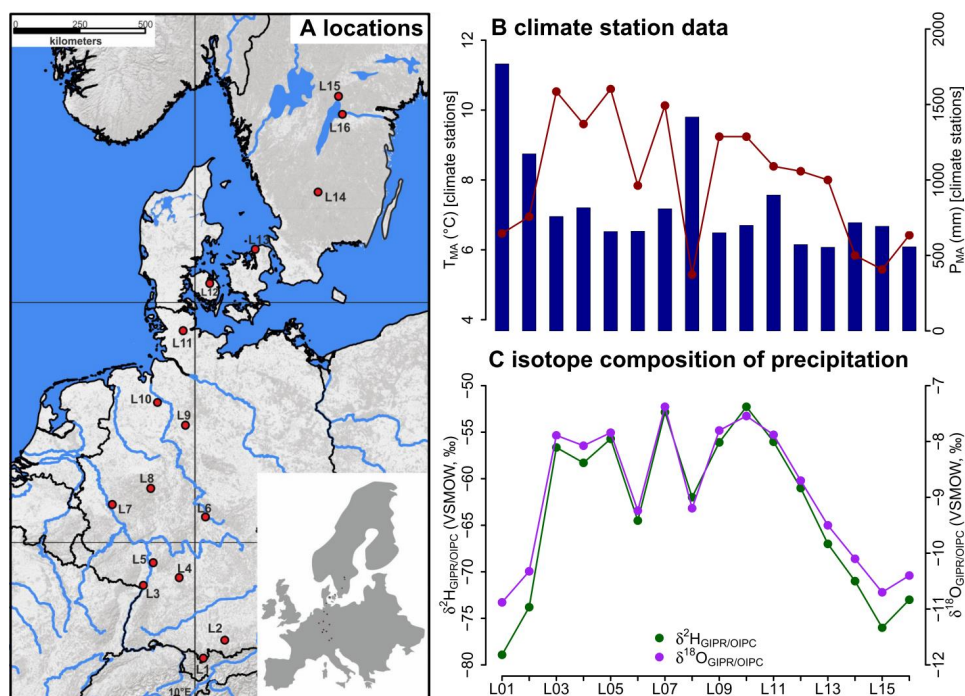
128 For comprising German precipitation $\delta^2\text{H}/\delta^{18}\text{O}$ along the transect, we realized a regionalisation
129 (called $\delta^2\text{H}/\delta^{18}\text{O}_{\text{GIPR}}$) using online available data from 34 German GNIP stations, 4 Austrian
130 ANIP stations and the Groningen GNIP station (van Geldern et al., 2014; IAEA/WMO, 2018;
131 Stumpp et al., 2014; Umweltbundesamt GmbH, 2018), following the approach of Schlotter
132 (2007). However, instead of the multivariate regression procedure applied by Schlotter (2007),
133 we used a random forest approach (Hothorn et al., 2006; Strobl et al., 2007, 2008) to describe
134 the relationship of squared latitude, latitude, longitude and altitude vs. long term weighted
135 means of precipitation $\delta^2\text{H}/\delta^{18}\text{O}$, and realized the prediction for the study sites. For the Danish



136 and Swedish sites, such a procedure was not possible. Hence, the annual precipitation $\delta^2\text{H}/\delta^{18}\text{O}$
137 values were derived from the Online Isotopes in Precipitation Calculator (OIPC, version 3.1),
138 therefore called $\delta^2\text{H}/\delta^{18}\text{O}_{\text{OIPC}}$ (Bowen, 2018; Bowen and Revenaugh, 2003; IAEA/WMO,
139 2015). The finally used $\delta^2\text{H}/\delta^{18}\text{O}_{\text{GIPR/OIPC}}$ data are given in Tab. S1.

140 The T_{MA} along the transect ranges from 5.3 to 10.6°C, and P_{MA} ranges from 554 to 1769 mm
141 (Fig. 1B). Precipitation $\delta^2\text{H}/\delta^{18}\text{O}$ shows moderate changes along the transect, $\delta^2\text{H}_{\text{GIPR/OIPC}}$
142 varies between -52 and -79‰, and $\delta^{18}\text{O}_{\text{GIPR/OIPC}}$ ranges from -7.4 to -10.9‰ (Fig. 1C).

143 Correlations between $\delta^{18}\text{O}_{\text{GIPR/OIPC}}$ and P_{MA} , altitude of the locations, T_{MA} are given in the
144 supplementary material (Fig. S1 to S3), along with a $\delta^2\text{H}_{\text{GIPR/OIPC}}$ vs. $\delta^{18}\text{O}_{\text{GIPR/OIPC}}$ scatter plot
145 (Fig. S4).



146 **Fig. 1.** (A) Sample locations (red dots, map source: US National Park Service), (B) variations
147 of mean annual air temperature (T_{MA}) and mean annual precipitation (P_{MA}) derived from close-
148 by climate station data, and (C) hydrogen and oxygen stable isotope composition of
149 precipitation ($\delta^2\text{H}_{\text{GIPR/OIPC}}$ and $\delta^{18}\text{O}_{\text{GIPR/OIPC}}$, respectively) as derived for the sampled transect
150 locations (see section 2.2 GIPR $\delta^2\text{H}/\delta^{18}\text{O}$ generation procedure). The reader is referred to
151 section 2.2 (and Tab. S1 and S2) for database and reference information of data plotted in (B)
152 and (C).
153

154

155 2.3 Soil extractions and analysis

156 2.3.1 GDGTs and pH

157 A detailed description of sample preparation for lipid analysis can be found in Schäfer et al.
158 (2016). Briefly, 1–6 g freeze-dried and grounded soil sample was microwave extracted with 15



159 ml dichloromethane (DCM)/methanol (MeOH) 9:1 (*v:v*) at 100°C for 1 h. Extracts were
160 separated over aminopropyl silica gel (Supelco, 45 µm) pipette columns. The nonpolar fraction
161 (including *n*-alkanes) was eluted with hexane and further purified over AgNO₃ coated silica
162 pipette columns (Supelco, 60-200 mesh) and zeolite (Geokleen Ltd.). The GDGT-containing
163 fraction was eluted with DCM:MeOH 1:1 (*v:v*), re-dissolved in hexane/isopropanol (IPA) 99:1
164 (*v:v*) and transferred over 0.45 µm PTFE filters into 300 µl inserts. For quantification, a known
165 amount of a C₄₆ diol standard was added after transfer. The samples were analysed at ETH
166 Zurich using an Agilent 1260 Infinity series HPLC–atmospheric chemical pressure ionization
167 mass spectrometer (HPLC–APCI-MS) equipped with a Grace Prevail Cyano column (150 mm
168 × 2.1 mm; 3 µm). The GDGTs were eluted isocratically with 90% A and 10% B for 5 min and
169 then with a linear gradient to 18% B for 34 min at 0.2 ml min⁻¹, where A=hexane and
170 B=hexane/isopropanol (9:1, *v:v*). Injection volume was 10 µl and single ion monitoring of
171 [M+H]⁺ was used to detect GDGTs.

172 The pH of the samples was measured in the laboratory of the Soil Biogeochemistry group,
173 Institute of Agronomy and Nutritional Sciences, Martin-Luther-University Halle-Wittenberg,
174 in a 1:3 soil:water (*w/v*) mixture.

175

176 2.3.2 δ²H_{*n*-alkane}

177 The hydrogen isotopic composition of the highest concentrated *n*-alkanes (*n*-C₂₅, *n*-C₂₇, *n*-C₂₉,
178 *n*-C₃₁, and *n*-C₃₃) was determined using a TRACE GC Ultra Gas Chromatography connected to
179 a Delta V Plus Isotope Ratio Mass Spectrometer via a ²H pyrolysis reactor (GC-²H-Py-IRMS;
180 Thermo Scientific, Bremen, Germany) at the ETH Zurich. The compound-specific ²H/¹H ratios
181 were calibrated against an external standard with C₁₅ – C₃₅ homologues. External standard
182 mixtures (A4 mix from A. Schimmelmann, University of Indiana) were run between the
183 samples for multipoint linear normalization. The H⁺³ factor was determined on each
184 measurement day and was constant throughout the periods of the sample batches. Samples were
185 analysed in duplicates, and results typically agreed within 4% (average difference = 1.4%). All
186 δ²H values are expressed relative to the Vienna Standard Mean Ocean Water (V-SMOW).

187

188 2.3.3 δ¹⁸O_{sugar}

189 Hemicellulose sugars were extracted and purified using a slightly modified standard procedure
190 (Amelung et al., 1996; Guggenberger et al., 1994; Zech and Glaser, 2009). Briefly, myoinositol
191 was added to the samples prior to extraction as first internal standard. The sugars were released
192 hydrolytically using 4M trifluoroacetic acid for 4 h at 105°C, cleaned over glass fiber filters and
193 further purified using XAD and Dowex columns. Before derivatization with methylboronic acid
194 (Knapp, 1979), the samples were frozen, freeze-dried, and 3-O-methylglucose in dry pyridine
195 was added as second internal standard. Compound-specific hemicellulose sugar ¹⁸O
196 measurements were performed in the laboratory of the Soil Biogeochemistry group, Institute of
197 Agronomy and Nutritional Sciences, Martin-Luther-University Halle-Wittenberg, using GC-
198 ¹⁸O-Py-IRMS (all devices from Thermo Fisher Scientific, Bremen, Germany). Standard
199 deviations of the triplicate measurements were 1.4‰ (over 29 investigated samples) for
200 arabinose and xylose, respectively. We focus on these two hemicellulose-derived neutral sugars



201 arabinose and xylose as they strongly predominate over fucose in terrestrial plants, soils and
202 sediments (Hepp et al., 2016 and references therein). Rhamnose concentrations were too low to
203 obtain reliable $\delta^{18}\text{O}$ results. All $\delta^{18}\text{O}$ values are expressed relative to the Vienna Standard Mean
204 Ocean Water (V-SMOW).

205

206 2.4 Theory and Calculations

207 2.4.1 Calculations used for the GDGT-based reconstructions

208 The branched and isoprenoid tetraether (BIT) index is calculated according to Hopmans et al.
209 (2004), for structures see Fig. S5:

$$210 \quad \text{BIT} = \frac{\text{Ia} + \text{IIa} + \text{IIIa}}{\text{Ia} + \text{IIa} + \text{IIIa} + \text{crenarchaeol}} \quad (1)$$

211 The cyclopentane moiety number of brGDGTs correlates negatively with soil pH (Weijers et
212 al., 2007), which led to the development of the cyclization of branched tetraethers (CBT) ratio.
213 CBT and the CBT based pH (pH_{CBT}) were calculated according to Peterse et al. (2012):

$$214 \quad \text{CBT} = -\log \frac{\text{Ib} + \text{IIb}}{\text{Ia} + \text{IIa}} \quad (2)$$

$$215 \quad \text{pH}_{\text{CBT}} = 7.9 - 1.97 \times \text{CBT} \quad (3)$$

216 The number of methyl groups in brGDGTs correlates negatively with T_{MA} and soil pH (Peterse
217 et al., 2012; Weijers et al., 2007). Thus, the ratio of the methylation of branched tetraethers
218 (MBT) ratio and the CBT ratio can be used to reconstruct T_{MA} . We use the equation given by
219 Peterse et al. (2012):

$$220 \quad \text{MBT}' = \frac{\text{Ia} + \text{Ib} + \text{Ic}}{\text{Ia} + \text{Ib} + \text{Ic} + \text{IIa} + \text{IIb} + \text{IIc} + \text{IIIa}} \quad (4)$$

$$221 \quad T_{\text{MA}} = 0.81 - 5.67 \times \text{CBT} + 31.0 \times \text{MBT}' \quad (5)$$

222

223 2.4.2 Calculations and concepts used for the coupled $\delta^2\text{H}$ - $\delta^{18}\text{O}$ approach

224 The apparent fractionation is calculated according to Cernusak et al. (2016):

$$225 \quad \varepsilon_{n\text{-alkane}/\text{precipitation}} = \left(\frac{\delta^2\text{H}_{n\text{-alkane}} - \delta^2\text{H}_{\text{GIPR/OIPC}}}{1 + \delta^2\text{H}_{\text{GIPR/OIPC}}/1000} \right) \quad (6)$$

$$226 \quad \varepsilon_{\text{sugar}/\text{precipitation}} = \left(\frac{\delta^{18}\text{O}_{\text{sugar}} - \delta^{18}\text{O}_{\text{GIPR/OIPC}}}{1 + \delta^{18}\text{O}_{\text{GIPR/OIPC}}/1000} \right) \quad (7)$$

227 The isotopic composition of leaf water ($\delta^2\text{H}/\delta^{18}\text{O}_{\text{leaf water}}$) can be calculated using ε_{bio} for $\delta^2\text{H}_{n\text{-}}$
228 alkane (-160‰, Sachse et al., 2012; Sessions et al., 1999) and $\delta^{18}\text{O}_{\text{sugar}}$ (+27‰, Cernusak et al.,
229 2003; Schmidt et al., 2001):

$$230 \quad \delta^2\text{H}_{\text{leaf water}} = \left(\frac{1000 + \delta^2\text{H}_{n\text{-alkane}}}{1000 + \varepsilon_{\text{bio}}(n\text{-alkane})} \right) \times 10^3 - 1000, \quad (8)$$

$$231 \quad \delta^{18}\text{O}_{\text{leaf water}} = \left(\frac{1000 + \delta^{18}\text{O}_{\text{sugar}}}{1000 + \varepsilon_{\text{bio}}(\text{sugar})} \right) \times 10^3 - 1000. \quad (9)$$

232 Zech et al. (2013) introduced the conceptual model for the coupled $\delta^2\text{H}_{n\text{-alkane}} - \delta^{18}\text{O}_{\text{sugar}}$ approach
233 in detail. Briefly, the coupled approach is based on the following assumptions (illustrated in
234 Fig. 8): (i) The isotopic composition of precipitation, which is set to be equal to the plant source
235 water, typically plots along the global meteoric water line (GMWL; $\delta^2\text{H} = 8 \times \delta^{18}\text{O} + 10$) in a



236 $\delta^{18}\text{O}$ vs. $\delta^2\text{H}$ space (Craig, 1961); (ii) Source water uptake by plants does not lead to any
237 fractionation (e.g. Dawson et al., 2002), and significant evaporation of soil water can be
238 excluded; (iii) Evapotranspiration leads to enrichment of the remaining leaf water along the
239 local evaporation line (LEL; Allison et al., 1985; Bariac et al., 1994; Walker and Brunel, 1990),
240 compared to the source water taken up by the plant; (iv) The biosynthetic fractionation is
241 assumed to be constant. In addition, isotopic equilibrium between plant source water (~
242 weighted mean annual precipitation) and the local atmospheric water vapour is assumed.
243 Further assumption concerns the isotope steady-state in the evaporating leaf water reservoir.
244 The coupled approach allows for reconstructing the isotopic composition of plant source water
245 ($\delta^2\text{H}/\delta^{18}\text{O}_{\text{source-water}}$) from the reconstructed leaf water, by calculating the intercepts of the LELs
246 with the GMWL (Zech et al., 2013). The slope of the LEL (S_{LEL}) can be assessed by the
247 following equation (Gat, 1971):

$$248 \quad S_{\text{LEL}} = \frac{\varepsilon_2^* + C_k^2}{\varepsilon_{18}^* + C_k^{18}}, \quad (10)$$

249 where ε^* are equilibrium isotope fractionation factors and C_k are kinetic fractionation factors.
250 The latter equals to 25.1‰ and 28.5‰, for C_k^2 and C_k^{18} , respectively (Merlivat, 1978). The
251 equilibrium fractionation factors can be derived from empirical equations (Horita and
252 Wesolowski, 1994) by using T_{MDV} values. For two Danish sites T_{MDV} are not available, instead
253 T_{MV} is used here (section 2.2 and Tab. S2).

254 In a $\delta^{18}\text{O}$ - $\delta^2\text{H}$ diagram, the distance of the leaf water from the GMWL define the deuterium-
255 excess of leaf water ($d_{\text{leaf-water}} = \delta^2\text{H}_{\text{leaf-water}} - 8 \times \delta^{18}\text{O}_{\text{leaf-water}}$, according Dansgaard, (1964); Fig.
256 8). To convert $d_{\text{leaf-water}}$ into mean RH during daytime and vegetation period (RH_{MDV}), a
257 simplified Craig-Gordon model can be applied (Zech et al., 2013):

$$258 \quad \text{RH} = 1 - \frac{\Delta d}{\varepsilon_2^* - 8 \times \varepsilon_{18}^* + C_k^2 - 8 \times C_k^{18}}, \quad (11)$$

259 where Δd is the difference in $d_{\text{leaf-water}}$ and the deuterium-excess of source water ($d_{\text{source-water}}$).

260

261 2.5 Statistics

262 In the statistical analysis we checked sample distributions for normality (Shapiro and Wilk,
263 1965) and for equal variance (Levene, 1960). If normality and equal variances are given, we
264 perform an Analysis of Variance (ANOVA). If that is not the case, we conduct the non-
265 parametric Kruskal-Wallis Test. ANOVA or Kruskal-Wallis are used to find significant
266 differences ($\alpha=0.05$) between the vegetation types (deciduous, conifer and grass).

267 In order to describe the relation along a 1:1 line, the coefficient of correlation (R^2) was
268 calculated as $R^2 = 1 - \frac{\sum(\text{modeled} - \text{measured})^2}{\sum(\text{measured} - \text{measured mean})^2}$. The small
269 r^2 is taken as coefficient of correlation of a linear regression between a dependent (y) and
270 explanatory variable(s). The root mean square error (RMSE) of the relationships was calculated

271 as $\text{RMSE} = \sqrt{\left(\frac{1}{n} \cdot \sum(\text{modeled} - \text{measured})^2\right)}$. All data plotting and statistical analysis was
272 realized in R (version 3.2.2; R Core Team, 2015).

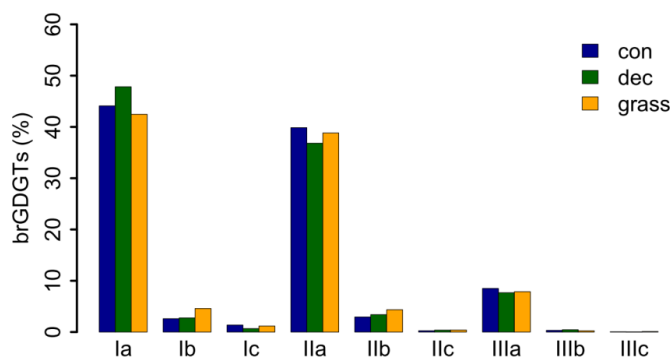
273



274 **3 Results and Discussion**

275 **3.1 GDGT concentrations**

276 GDGT Ia has the highest concentration under all vegetation types, followed by GDGT IIa and
277 GDGT IIIa (Fig. 2). GDGT Ib, IIb and Ic occur in minor, GDGT IIc and IIIb only in trace
278 amounts. GDGT IIIc was below the detection limit in most of the samples (Tab. S3). Although
279 other studies document an influence of the vegetation cover on soil temperature and soil water
280 content, which control the microbial community composition in soils (Awe et al., 2015; Liu et
281 al., 2014; Mueller-Niggemann et al., 2016), we find no statistically different pattern of the
282 individual brGDGTs.



283

284 **Fig. 2.** Mean concentrations of individual brGDGTs as percentage of all brGDGTs for the three
285 investigated types. Abbreviations: con = coniferous forest sites (n=9); dec = deciduous forest
286 sites (n=14); grass = grassland sites (n=6).

287 Total concentrations of brGDGTs range from 0.32 to 9.17 $\mu\text{g/g}$ dry weight and tend to be
288 highest for the coniferous samples and lowest for the grasses (Fig. 3A, Tab. S3). Bulk brGDGT
289 concentrations lie within ranges of other studies examining soils of mid latitude regions (Huguet
290 et al., 2010b, 2010a; Weijers et al., 2011). Similar concentrations in coniferous and deciduous
291 samples imply that brGDGT production does not strongly vary in soils below different forest
292 types. The grass samples show lower brGDGT concentrations compared to the forest samples,
293 but this is probably mainly due to ploughing of the grass sites and hence admixing of mineral
294 subsoil material. Anyhow, the differences in brGDGT concentrations are not significant (p-
295 value = 0.06).

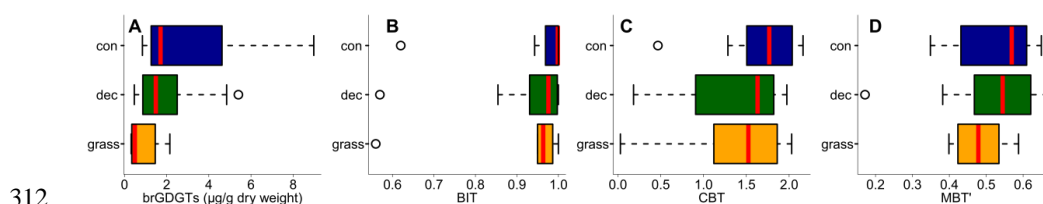
296

297 **3.2 BIT index**

298 Most of the samples have a BIT index higher than 0.9 (Fig 3B and Tab. S3). The BIT-values
299 are typical for soils in humid and temperate climate regions (Weijers et al., 2006). However,
300 outliers exist. The most likely source of iGDGTs in soils are Thaumarchaeota, i.e. aerobic
301 ammonia oxidizing archaea producing Crenarchaeol and its regioisomer (Schouten et al., 2013
302 and references therein), precipitation amounts drop below 700-800 mm (Dang et al., 2016;
303 Dirghangi et al., 2013). The P_{MA} data of our sampling sites mostly show precipitation > 550
304 mm (Fig. 1B), but one has to be aware that this data is based on the climate station nearest to
305 the respective sampling locations and microclimate effects, such as sunlight exposure, canopy



306 cover or exposition might have a pronounced influence on the brGDGT vs. iGDGT distribution.
307 Mueller-Niggemann et al. (2016) found higher BIT indices in upland soils compared to paddy
308 soils and stated that the management type also influences BIT values in soils. Along our
309 transect, grass sites tend to have slightly lower BIT-values than forest sites, probably due to the
310 absence of a litter layer and hence, no isolation mechanism preventing evaporation of soil water.
311 Anyhow, differences between vegetation types are not significant (p -value = 0.32).



312

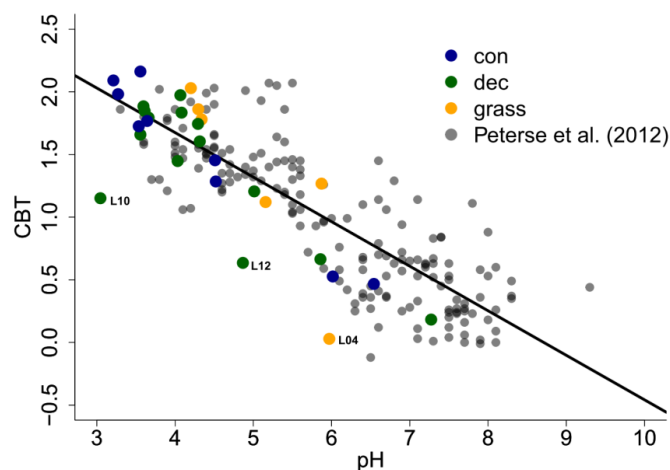
313 **Fig. 3.** (A) Total concentrations of brGDGTs in $\mu\text{g g}^{-1}$ dry weight, as well as (B) BIT, (C) CBT
314 and (D) MBT'. Abbreviations: con = coniferous forest sites ($n=9$); dec = deciduous forest sites
315 ($n=14$); grass = grassland sites ($n=6$). Box plots show median (red line), interquartile range
316 (IQR) with upper (75%) and lower (25%) quartiles, lowest whisker still within 1.5IQR of lower
317 quartile, and highest whisker still within 1.5IQR of upper quartile, dots mark outliers.

318

319 3.3 CBT-derived pH

320 The CBT ratio shows a pronounced variation independent of vegetation type with values
321 between 0.03 and 2.16 (Fig 3C). The coniferous samples tend to be highest, but the differences
322 between vegetation types are not significant (p -value = 0.48). The CBT index can be related to
323 pH in acidic and/or humid soils (e.g. Dirghangi et al., 2013; Mueller-Niggemann et al., 2016;
324 Peterse et al., 2012; Weijers et al., 2007) but might be an indicator of soil water content and
325 hence, precipitation in more arid and alkaline soils (e.g. Dang et al., 2016). There is a
326 pronounced correlation between CBT and soil pH (Fig. 4), which is in good agreement with
327 other studies from mid latitude regions where precipitation is relatively high (Anderson et al.,
328 2014 and references therein). Moreover, the CBT to pH relationship in terms of slope and
329 intersect in our dataset ($\text{CBT} = -0.47 \times \text{pH} + 3.5$, $r^2 = 0.7$, p -value < 0.0001, $n = 29$) is well
330 comparable to the correlation described for the global calibration dataset of Peterse et al. (2012)
331 ($\text{CBT} = -0.36 \times \text{pH} + 3.1$, $r^2 = 0.7$, p -value < 0.0001, $n = 176$).

332 However, there are some outliers in the CBT-pH correlation, which need a further examination
333 (see locations grass L04, dec L10 and dec L12 as marked in Figs. 4 and 5). The outliers show
334 lower BIT indices (< 0.85, Tab. S3). Even though the data from the nearest climate station
335 suggest no abnormal P_{MA} . Local effects such as differences in the amount of sunlight exposure,
336 nutrient availability for brGDGT producing organisms or, most likely soil water content might
337 influence the brGDGT production at these locations (Anderson et al., 2014; Dang et al., 2016).
338 A lower BIT index as well as a lower CBT occur when soil water content decreases (Dang et
339 al., 2016; Sun et al., 2016) or when aeration is high and less anoxic microhabitats for GDGT
340 producing microbes exist (e.g. Dirghangi et al., 2013).

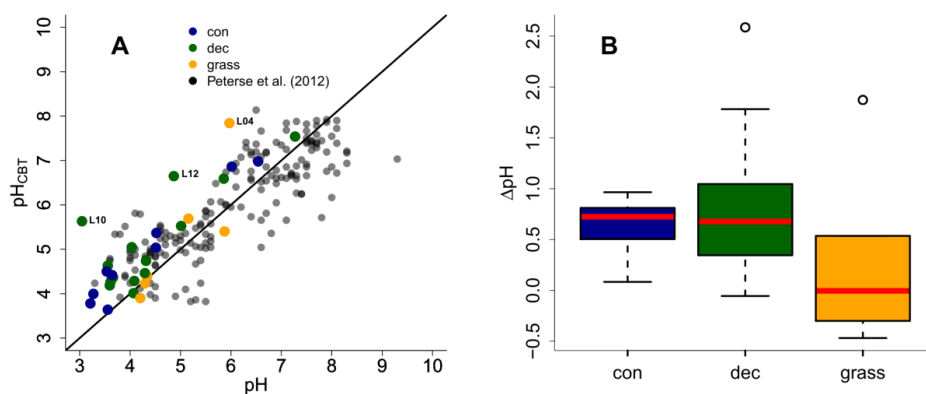


341

342 **Fig. 4.** CBT to pH relationship in our dataset in comparison to the global calibration dataset
343 from Peterse et al. (2012) ($CBT = -0.36 \times pH + 3.1$, $r^2 = 0.7$, p -value < 0.0001 , $n = 176$, black
344 line). Abbreviations: con = coniferous forest sites ($n=9$); dec = deciduous forest sites ($n=14$);
345 grass = grassland sites ($n=6$).

346

347 As the CBT and pH are similarly correlated in our dataset and the global dataset of Peterse et
348 al. (2012), the CBT-derived pH correlated well with the actual pH (Fig. 5A; $R^2 = 0.3$).
349 Expressed as ΔpH (CBT-derived pH - measured pH), there is a tendency that the GDGTs result
350 in an overestimation of the real pH for the forest sites (Fig. B). Yet a Kruskal-Wallis test shows
351 no statistically significant difference between the vegetation types, with a p -value of 0.13. The
352 overall ΔpH of 0.6 ± 0.6 shows that the reconstruction of soil pH using brGDGTs works well
353 along this transect.



354

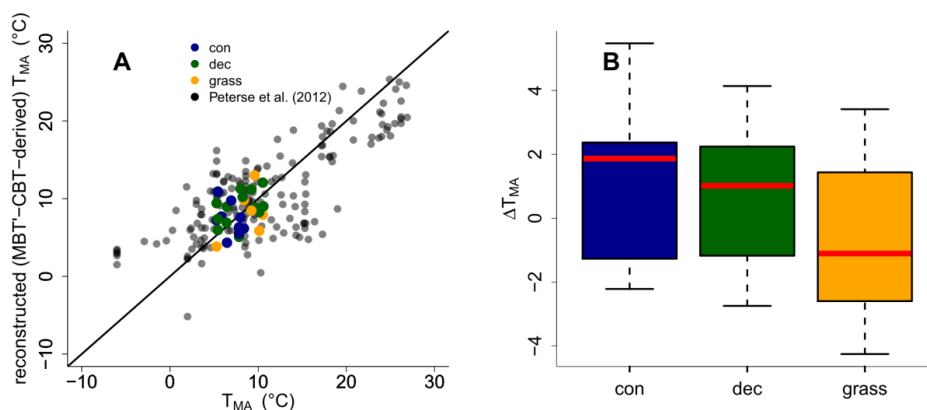
355 **Fig. 5.** (A) Correlation between measured pH and reconstructed soil pH (pH_{CBT}) from our
356 transect data in comparison to the global calibration dataset from Peterse et al. (2012) ($R^2 = 0.7$,
357 $RMSE = 0.75$, $n = 176$). Black line indicates the 1:1 relationship. (B) Boxplots of ΔpH (refers
358 to $pH_{CBT}-pH$). Box plots show median (red line), interquartile range (IQR) with upper (75%)



359 and lower (25%) quartiles, lowest whisker still within 1.5IQR of lower quartile, and highest
360 whisker still within 1.5IQR of upper quartile, dots mark outliers. Abbreviations: con =
361 coniferous forest sites (n=9); dec = deciduous forest sites (n=14); grass = grassland sites (n=6).
362

363 3.4 MBT'-CBT-derived T_{MA} reconstructions

364 The MBT' shows high variability with values ranging from 0.17 to 0.67 no statistical
365 differences between vegetation types (p-value = 0.54; Fig. 3D, Tab. S3). When comparing
366 reconstructed (MBT'-CBT-derived) T_{MA} with climate station T_{MA} , the data plot close to the 1:1
367 line, and fit well into the global dataset of Peterse et al. (2012) (Fig. 7A). The ΔT_{MA} reveal an
368 overall offset of $0.5^{\circ}\text{C} \pm 2.4$ and there is no statistically difference between vegetation types
369 (Fig. 7B). The standard deviation in ΔT_{MA} of ± 2.4 is well in line with the RMSE of 5.0 for the
370 global calibration dataset (Peterse et al., 2012).



371
372 **Fig. 6.** (A) Correlation between climate station T_{MA} and reconstructed (MBT'-CBT-derived)
373 T_{MA} . For comparison, the global calibration dataset from Peterse et al. (2012) is shown. The
374 black line indicates the 1:1 relationship. (B) Boxplots of ΔT_{MA} (refers to reconstructed T_{MA} -
375 T_{MA} from climate stations) in the different vegetation types from our transect study. Box plots
376 show median (red line), interquartile range (IQR) with upper (75%) and lower (25%) quartiles,
377 lowest whisker still within 1.5IQR of lower quartile, and highest whisker still within 1.5IQR of
378 upper quartile, dots mark outliers. Abbreviations: con = coniferous forest sites (n=9); dec =
379 deciduous forest sites (n=14); grass = grassland sites (n=6).

380

381 3.5 Apparent fractionation of $\delta^2\text{H}$ and $\delta^{18}\text{O}$ in the different vegetation types

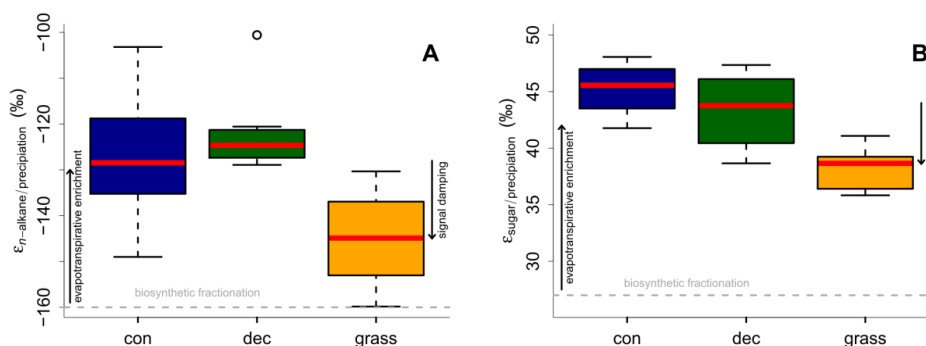
382 The $\delta^2\text{H}$ values could be obtained for *n*-alkanes C_{27} , C_{29} and C_{31} in all samples and additionally
383 at two locations for *n*- C_{25} and *n*- C_{33} at six other locations. The $\delta^2\text{H}_{n\text{-alkane}}$ values, calculated as
384 mean of *n*- C_{25} to *n*- C_{31} $\delta^2\text{H}$, ranges from -156 to -216‰. Pooled standard deviations show an
385 overall average of 3.6‰. The $\delta^{18}\text{O}_{\text{sugar}}$ values, calculated as the area weighted means for
386 arabinose and xylose, ranges from 27.7 to 39.4‰. The average weighted mean standard
387 deviation is 1.4‰. The compound-specific isotope data is summarized along with the
388 calculations in Tab. S4.



389 Apparent fractionation ($\epsilon_{n\text{-alkane/precipitation}}$) is on the order of -120 to -150‰, i.e. a bit less than
390 the biosynthetic fraction of -160‰. This implies that evapotranspirative enrichment is ~ 10 to
391 40‰ (Fig. 7A). $\epsilon_{n\text{-alkane/precipitation}}$ is lower for grass sites compared to the forest sites. Differences
392 are significant between deciduous and grass sites (p-value = 0.005). This finding supports the
393 results of other studies (Kahmen et al., 2013; Liu and Yang, 2008; McInerney et al., 2011), and
394 can be named “signal damping”. Grasses do not only incorporate the evaporatively-enriched
395 leaf water only but also unenriched leaf water in the growth and differentiation zone of grasses
396 (Gamarra et al., 2016; Liu et al., 2017).

397 The grass-derived hemicellulose sugar biomarkers do not fully record the evapotranspirative
398 enrichment of the leaf water, either, as indicated by lower apparent fractionation ($\epsilon_{\text{sugar/precipitation}}$)
399 in Fig. 7B. The differences are significant between forest and grass sites (p-value < 0.005). This
400 is in agreement with a study on cellulose extracted from grass blades (Helliker and Ehleringer,
401 2002), and again, the “signal damping” can be explained with incorporation of enriched leaf
402 water and non-enriched stem water.

403 Based on the comparison of evapotranspirative enrichment between forest and grass sites, the
404 “signal damping” can be quantified to be ~ 31% for the hemicellulose sugars, and ~ 49% for
405 the *n*-alkanes. This is in agreement with other studies that reported a loss of 22% of the leaf
406 water enrichment for hemicellulose sugars (Helliker and Ehleringer, 2002) and 39 to 62% loss
407 of the leaf water enrichment for *n*-alkanes (Gamarra et al., 2016).



408
409 **Fig. 7.** Apparent fractionation (A) $\epsilon_{n\text{-alkane/precipitation}}$ and (B) $\epsilon_{\text{sugar/precipitation}}$. Biosynthetic
410 fractionation factors according to section 2.4.2. Box plots show median (red line), interquartile
411 range (IQR) with upper (75%) and lower (25%) quartiles, lowest whisker still within 1.5IQR
412 of lower quartile, and highest whisker still within 1.5IQR of upper quartile, dots mark outliers.
413 Abbreviations: con = coniferous forest sites (n=9); dec = deciduous forest sites (n=11 and 14
414 for *n*-alkanes and sugars, respectively); grass = grassland sites (n=4 and 6 for *n*-alkanes and
415 sugars, respectively). The figure conceptually illustrates the effect of biosynthetic fractionation
416 and evapotranspirative enrichment as well as “signal damping”.

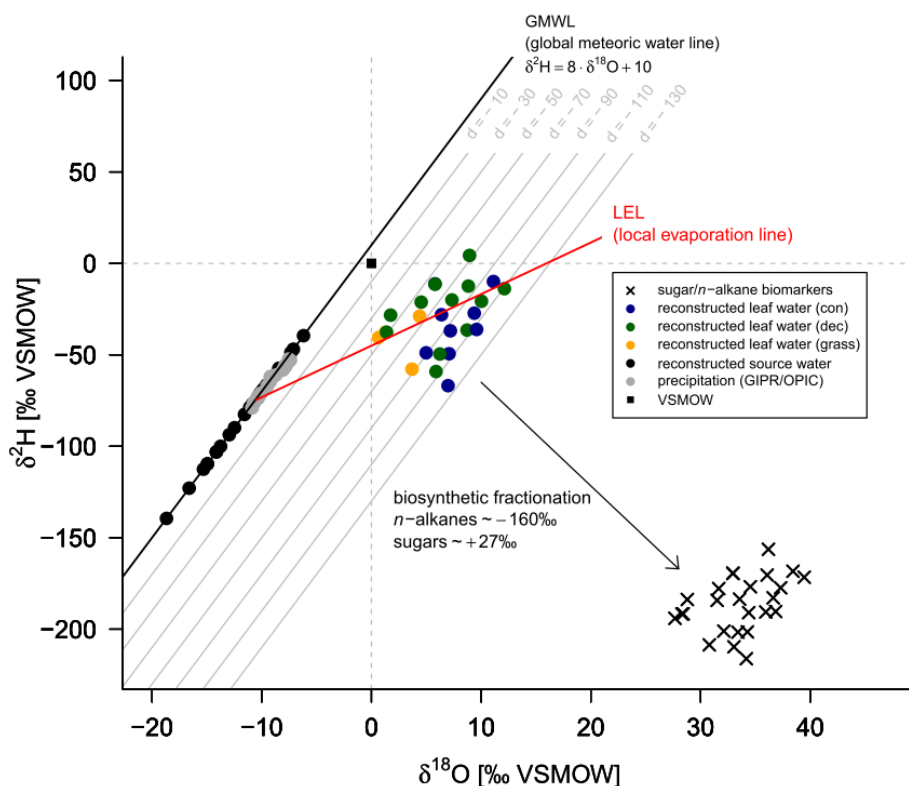
417

418 3.6 $\delta^2\text{H}/\delta^{18}\text{O}_{\text{source-water}}$ reconstructions

419 The $\delta^2\text{H}$ versus $\delta^{18}\text{O}$ diagram shown in Fig. 8 graphically illustrates the reconstruction of
420 $\delta^2\text{H}/\delta^{18}\text{O}_{\text{leaf-water}}$ (colored dots) from $\delta^2\text{H}_{n\text{-alkane}}/\delta^{18}\text{O}_{\text{sugar}}$ (crosses), as well as the reconstruction



421 of $\delta^2\text{H}/\delta^{18}\text{O}_{\text{source-water}}$ (black dots). For reconstructing $\delta^2\text{H}/\delta^{18}\text{O}_{\text{source-water}}$, LELs with an average
 422 slope of 2.8 ± 0.1 (Eq. 10) can be generated through every leaf water point and the intercepts of
 423 these LELs with the GMWL.



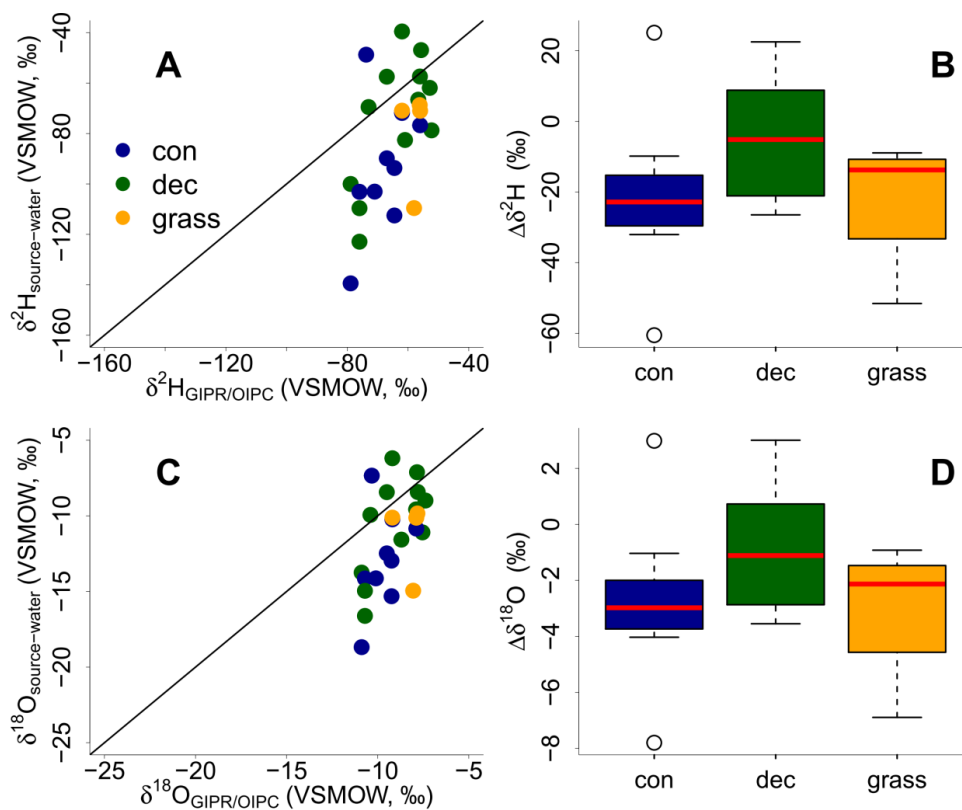
424
 425 **Fig. 8.** $\delta^2\text{H}$ vs. $\delta^{18}\text{O}$ diagram illustrating $\delta^2\text{H}_{n\text{-alkane}}$ and $\delta^{18}\text{O}_{\text{sugar}}$, reconstructed $\delta^2\text{H}/\delta^{18}\text{O}_{\text{leaf-water}}$
 426 (according Eqs. 8 and 9) and reconstructed $\delta^2\text{H}/\delta^{18}\text{O}_{\text{source-water}}$ in comparison to GIPR/OIPC-
 427 based $\delta^2\text{H}/\delta^{18}\text{O}_{\text{precipitation}}$. Abbreviations: con = coniferous forest sites (n=9); dec = deciduous
 428 forest sites (n=11); grass = grassland sites (n=4).

429
 430 The reconstructed $\delta^2\text{H}/\delta^{18}\text{O}_{\text{source-water}}$ results can be compared with the $\delta^2\text{H}/\delta^{18}\text{O}_{\text{GIPR/OIPC}}$ data
 431 (Fig. 9). This comparison reveals that the coupled $\delta^2\text{H}_{n\text{-alkane}}-\delta^{18}\text{O}_{\text{sugar}}$ approach yields more
 432 accurate $\delta^2\text{H}/\delta^{18}\text{O}_{\text{source-water}}$ results than hitherto applied $\delta^2\text{H}_{n\text{-alkane}}$ single isotope approaches.
 433 However, the range of the reconstructed $\delta^2\text{H}/\delta^{18}\text{O}_{\text{source-water}}$ values is clearly larger than in
 434 $\delta^2\text{H}/\delta^{18}\text{O}_{\text{GIPR/OIPC}}$ values. $\delta^2\text{H}$ is systematically underestimated by $\sim 21\text{‰} \pm 22$ (Fig. 9B) and
 435 $\delta^{18}\text{O}$ by $\sim 2.9\text{‰} \pm 2.8$ (Fig. 9D). The type of vegetation seems to be not particularly relevant (p-
 436 value = 0.18 for $\Delta\delta^2\text{H}$ and p-value = 0.34 for $\Delta\delta^{18}\text{O}$). Nevertheless, the systematic offsets tend
 437 to be lowest for the deciduous sites ($\Delta\delta^2\text{H}/\Delta\delta^{18}\text{O}$ is closer to zero with $\sim -5\text{‰} \pm 15$ and $\sim -1.1\text{‰}$
 438 ± 2.1), followed by grass sites ($\sim -14\text{‰} \pm 20$ and $\sim -2.1\text{‰} \pm 2.6$). In comparison, the coniferous
 439 sites show the largest offsets ($\sim -23\text{‰} \pm 26$ for $\Delta\delta^2\text{H}$ $\sim -3.0\text{‰} \pm 3.3$ for $\Delta\delta^{18}\text{O}$). Differences are,
 440 however, not statistically significant. The systematic offset and the large variability might have



441 more specific reasons, and we suggest that this is related to the type of vegetation. Deciduous
442 trees produce lots of leaf waxes and sugars (e.g. Prietzel et al., 2013; Zech et al., 2012a), and
443 all biomarkers reflect and record the evapotranspirative enrichment of the leaf water (e.g.
444 Cernusak et al., 2016; Tuthorn et al., 2014). The coupled approach and the leaf water
445 reconstruction based on the *n*-alkane and sugar biomarkers thus works well. However,
446 coniferous trees produce quite low amounts of *n*-alkanes (Diefendorf and Freimuth, 2016; Zech
447 et al., 2012a), while sugar concentrations are as high as in other vascular plants (e.g. Hepp et
448 al., 2016; Prietzel et al., 2013). For the coniferous soil samples this means that the *n*-alkanes
449 stem most likely from the understory whereas the sugars originate from grasses and coniferous
450 needles. When the understory is dominated by grass species then the *n*-alkane biomarkers do
451 not record the full leaf water enrichment signal, whereas the sugars from the needles do. The
452 reconstructed leaf water for the coniferous sites is therefore too negative concerning $\delta^2\text{H}$, and
453 reconstructed $\delta^2\text{H}/\delta^{18}\text{O}_{\text{source-water}}$ values thus also become too negative (Fig. 8). Concerning the
454 grass sites the following explanation can be found. Correcting for “signal damping” makes the
455 reconstructed leaf water points more positive and shifts them in Fig. 8 up and right. As the
456 “signal damping” is stronger for $\delta^2\text{H}$ than for $\delta^{18}\text{O}$ the corrected leaf water points are now above
457 the uncorrected ones. The corrected leaf water points leads to more positive reconstructed
458 $\delta^2\text{H}/\delta^{18}\text{O}_{\text{source-water}}$ values for the grass sites.

459 Vegetation type specific rooting depths could partly cause the overall high variability in
460 reconstructed $\delta^2\text{H}/\delta^{18}\text{O}_{\text{source-water}}$. Deep rooting species most likely use the water from deeper
461 soil horizons and/or shallow ground water, which is equal to the (weighted) mean annual
462 precipitation (e.g. Herrmann et al., 1987). Shallow rooting plants take up water from upper soil
463 horizons, which is influenced by seasonal variations in $\delta^2\text{H}/\delta^{18}\text{O}_{\text{precipitation}}$ and by soil water
464 enrichment (Dubbett et al., 2013). Thus, the overall assumption that the source water of the
465 plants reflects the local (weighted) mean precipitation might be not fully valid for all sites.
466 Moreover, a partly contribution of root-derived rather than leaf-derived sugar biomarkers in our
467 topsoil samples is very likely. This does, by contrast, not apply for *n*-alkanes, which are hardly
468 produced in roots (Zech et al., 2012b and the discussion).



469
470 **Fig. 9.** Correlation of reconstructed $\delta^2\text{H}/\delta^{18}\text{O}_{\text{source-water}}$ vs. precipitation $\delta^2\text{H}/\delta^{18}\text{O}_{\text{GIPR/OIPC}}$ (A and
471 C). Black lines indicate 1:1 relationship. Differences between reconstructed source water and
472 precipitation ($\Delta\delta^2\text{H}/\delta^{18}\text{O} = \delta^2\text{H}/\delta^{18}\text{O}_{\text{source-water}} - \delta^2\text{H}/\delta^{18}\text{O}_{\text{GIPR/OIPC}}$) for the three different
473 vegetation types (B and D). Box plots show median (red line), interquartile range (IQR) with
474 upper (75%) and lower (25%) quartiles, lowest whisker still within 1.5IQR of lower quartile,
475 and highest whisker still within 1.5IQR of upper quartile. Abbreviations: con = coniferous
476 forest sites (n=9); dec = deciduous forest sites (n=11); grass = grassland sites (n=4).

477 Moreover, the high variability within the vegetation types could be caused by variability in ϵ_{bio}
478 of ^2H in *n*-alkanes, as well as ^{18}O in sugars. There is an ongoing discussion about the correct
479 ϵ_{bio} for ^{18}O in hemicellulose sugars (Sternberg, 2014 vs. Zech et al., 2014), and ϵ_{bio} is probably
480 not constant over all vegetation types. This translates into errors concerning leaf water
481 reconstruction and thus for reconstructing $\delta^2\text{H}/\delta^{18}\text{O}_{\text{source-water}}$ values (Eq. 9 and Fig. 8).
482 Likewise, the ϵ_{bio} values reported in the literature for ^2H of *n*-alkanes can be off from -160‰
483 by tens of permille (Feakins and Sessions, 2010; Tipple et al., 2015; Feakins et al., 2016;
484 Freimuth et al., 2017). The degree to which hydrogen originates from NADPH rather than leaf
485 water is important, because NADPH is more negative (Schmidt et al., 2003). The wide range
486 in biosynthetic ^2H fractionation factors is therefore also related to the carbon and energy
487 metabolism state of plants (Cormier et al., 2018).

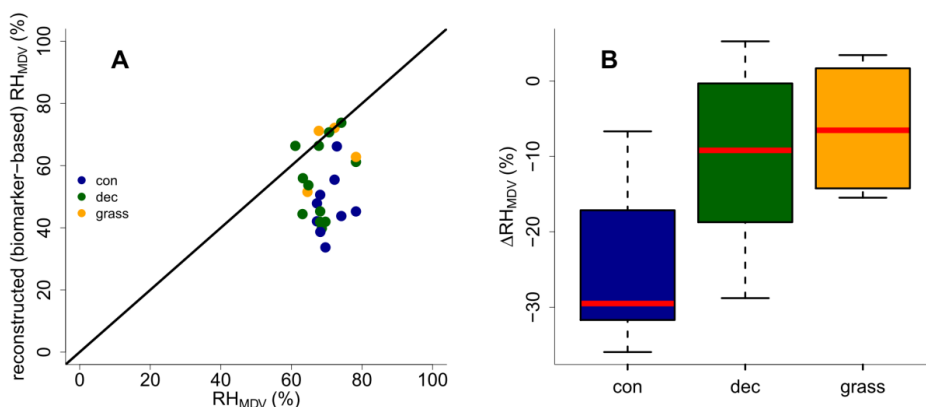


488 3.7 RH reconstruction

489 Reconstructed RH_{MDV} ranges from 34 to 74%, while RH_{MDV} from climate station data range
490 from 61 to 78% (Fig. 10A). Biomarker-based values thus systematically underestimate the
491 station data ($\Delta RH_{MDV} = -17\% \pm 12$; Fig. 10B). Yet the offsets are much less for deciduous tree
492 and grass sites ($\Delta RH_{MDV} = -10\% \pm 12$ and $-7\% \pm 9$, respectively). The offsets for the coniferous
493 sites are $-30\% \pm 11$, and significantly larger than for the deciduous and grass sites (p -values $<$
494 0.05).

495 Too low reconstructed RH_{MDV} values for the coniferous sites make sense in view of the
496 previously discussed option that soils contain n -alkanes from the understory (which is
497 dominated by grass species), while sugars stem from needles and grasses. As explained earlier
498 already, the “signal damping” leads to too negative reconstructed $\delta^2H_{leaf-water}$ (whereas $\delta^{18}O$ is
499 affected less by the “signal damping”), and too negative $\delta^2H_{leaf-water}$ translates into
500 overestimated d -excess and underestimated RH values. In Fig. 8, a correction for this require
501 moving the coniferous leaf water data points upwards towards more positive δ^2H values, thus
502 the distance between the leaf water and the source water is reduced.

503 The underestimation of RH for the deciduous and grass sites could be partly associated with the use
504 of the GMWL as baseline for the coupled $\delta^2H_{n-alkane}-\delta^{18}O_{sugar}$ approach. The deuterium-
505 excess of the LMWLs is generally lower than the $+10\%$ of the GMWL, while the slopes of the
506 LMWLs are well comparable to the GMWL (Stumpp et al., 2014). In addition, if soil water
507 evaporation occurred before water uptake by the plants, this would lead to an underestimation
508 of biomarker-based RH_{MDV} values. It can be furthermore assumed that plant metabolism is
509 highest during times with direct sunshine and high irradiation, i.e. during noon at sunny days.
510 The relevant RH could therefore be lower than the climate station-derived RH_{MDV} . Indeed,
511 already climate station RH_{MDV} is considerable lower than RH_{MA} and RH_{MV} (Tab. S1).



512

513 **Fig. 10.** (A) Comparison of reconstructed (biomarker-based) RH_{MDV} values and climate station
514 RH_{MDV} data. The black line indicates the 1:1 relationship. (B) Differences between
515 reconstructed and climate station RH_{MDV} values ($\Delta RH_{MDV} = \text{reconstructed} - \text{climate station}$
516 RH_{MDV}) for the three different vegetation types along the transect. Abbreviations: con =
517 coniferous forest sites (n=9); dec = deciduous forest sites (n=11); grass = grassland sites (n=4).



518 The uncertainty of reconstructed RH_{MDV} values are large for all three investigated vegetation
519 types, and again these uncertainties are probably also related to ϵ_{bio} , which is most likely not
520 constant as assumed for our calculations. Moreover, microclimate variability is underestimated
521 in our approach. As mentioned in sections 2.4.2 and 3.6, in the coupled approach not only the
522 source water of the plants is equated with (weighted) mean annual precipitation, but also an
523 isotopic equilibrium between the source water and the (local) atmospheric water vapour is
524 assumed. However, in areas with distinct seasonality this might be not fully valid. To account
525 for this lack of equilibrium between precipitation and local atmospheric water vapour, apparent
526 ϵ values can be calculated with data from Jacob and Sonntag, (1991). As shown by Hepp et al.
527 (2018) those values can be used to achieve alternative RH reconstructions based on the coupled
528 $\delta^2H_{n\text{-alkane}}\text{-}\delta^{18}O_{\text{sugar}}$ approach. Such calculated RH_{MDV} values are on average 1.5% more
529 negative than the original values. However, this difference in RH is far below the analytical
530 uncertainties of the compound-specific biomarker isotope analysis.

531 Finally, the integration time of the investigated topsoils has to be discussed. Unfortunately, no
532 ^{14}C dates are available for the soil samples. However, most likely the organic matter has been
533 built up over a longer timescale than the available climate data, which is used for comparison.
534 In combination with vegetation changes/management changes throughout that period, this
535 could surely lead to a less tight relationship of the reconstructions compared to the climate
536 station data. Root input of arabinose and xylose seems to be of minor relevance in our topsoil
537 samples. Otherwise, the reconstructed $\delta^{18}O_{\text{sugar}}$ values would be too negative resulting in
538 RH_{MDV} overestimations, which is not observed.

539

540 4 Conclusions

541 We were able to show that

- 542 (i) the vegetation type does not significantly influence the brGDGT concentrations and
543 proxies, yet the coniferous sites tend to have higher brGDGT concentrations, BIT
544 indices and CBT/MBT' ratios, while grass sites tend to be lowest.
- 545 (ii) CBT faithfully records soil pH with a median ΔpH of 0.6 ± 0.6 , The CBT
546 overestimates the real pH particularly at the forest sites.
- 547 (iii) CBT-MBT'-derived T_{MA} reflect the climate station-derived T_{MA} values with a
548 median ΔT_{MA} of $0.5^\circ C \pm 2.4$, but again slightly too high reconstruction for the forest
549 sites were observed.
- 550 (iv) differences in the apparent fractionation between the investigated vegetation types
551 are caused by "signal damping", i.e. the grasses do not see and record the full
552 evaporative enrichment of leaf water.
- 553 (v) the reconstructed $\delta^2H/\delta^{18}O_{\text{source-water}}$ reflects the $\delta^2H/\delta^{18}O_{GIPR/OIPC}$ with a systematic
554 offset for δ^2H of $\sim -21\text{‰} \pm 22$ and for $\delta^{18}O$ of $\sim -2.9\text{‰} \pm 2.8$ (based on overall medians
555 of $\Delta\delta^2H/\delta^{18}O$). This is caused by too negative reconstructions for coniferous and
556 grass sites. For coniferous sites, this can be explained with *n*-alkanes originating
557 from understory grasses, and for the grass sites the "signal damping" more effect
558 δ^2H than $\delta^{18}O$. This leads to too negative reconstructed $\delta^2H_{\text{leaf-water}}$ values and thus
559 to too negative $\delta^2H/\delta^{18}O_{\text{source-water}}$ reconstruction.



560 (vi) reconstructed (biomarker-based) RH_{MDV} values tend to underestimate climate
561 station-derived RH_{MDV} values ($\Delta RH_{MDV} = \sim -17\% \pm 12$). For coniferous sites the
562 underestimations are strongest, which can be explained with understory grasses
563 being the main source of *n*-alkanes for the investigated soils under coniferous
564 forests.

565 Overall, our study highlights the great potential of GDGTs and the coupled $\delta^2H_{n\text{-alkane}}\text{-}\delta^{18}O_{\text{sugar}}$
566 approach for more quantitative paleoclimate reconstructions. Taking into account effects of
567 different vegetation types improves correlations and reconstructions. This holds particularly
568 true for the coupled $\delta^2H_{n\text{-alkane}}\text{-}\delta^{18}O_{\text{sugar}}$ approach, which is affected by “signal damping” of the
569 grass vegetation. Assuming constant biosynthetic fractionation is likely a considerable source
570 of uncertainty. Climate chamber experiments would be very useful to further evaluate and refine
571 the coupled $\delta^2H_{n\text{-alkane}}\text{-}\delta^{18}O_{\text{sugar}}$ approach, because uncertainties related to microclimate
572 variability can be reduced. Field experiments like ours suffer from the fact that biomarker pools
573 in the sampled topsoils may have been affected by past vegetation and climate changes.

574

575 Acknowledgements

576 We thank L. Wüthrich, H. Veit, T. Sprafke, A. Groos (all University of Bern), A. Kühnel
577 (Technical University of Munich) for constructive discussions and statistical advices, and M.
578 Schaarschmidt (University of Bayreuth), C. Heinrich and M. Benesch (Martin-Luther-
579 University Halle-Wittenberg) for laboratory assistance during $\delta^{18}O_{\text{sugar}}$ analysis and pH
580 measurements, respectively. The Swiss National Science Foundation (PP00P2 150590) funded
581 this research. J. Hepp greatly acknowledges the support by the German Federal Environmental
582 Foundation (DBU) in form of his PhD-fellowship.

583

584 References

- 585 Allison, G. B., Gat, J. R. and Leaney, F. W. J.: The relationship between deuterium and oxygen-
586 18 delta values in leaf water, *Chemical Geology*, 58, 145–156, 1985.
- 587 Amelung, W., Cheshire, M. V. and Guggenberger, G.: Determination of neutral and acidic
588 sugars in soil by capillary gas-liquid chromatography after trifluoroacetic acid hydrolysis,
589 *Soil Biology and Biochemistry*, 28(12), 1631–1639, 1996.
- 590 Anderson, V. J., Shanahan, T. M., Saylor, J. E., Horton, B. K. and Mora, A. R.: Sources of local
591 and regional variability in the MBT/CBT paleotemperature proxy: Insights from a
592 modern elevation transect across the Eastern Cordillera of Colombia, *Organic
593 Geochemistry*, 69, 42–51, doi:10.1016/j.orggeochem.2014.01.022, 2014.
- 594 Awe, G. O., Reichert, J. M. and Wendroth, O. O.: Temporal variability and covariance
595 structures of soil temperature in a sugarcane field under different management practices
596 in southern Brazil, *Soil and Tillage Research*, 150, 93–106,
597 doi:10.1016/j.still.2015.01.013, 2015.
- 598 Bariac, T., Gonzalez-Dunia, J., Katerji, N., Béthenod, O., Bertolini, J. M. and Mariotti, A.:
599 Spatial variation of the isotopic composition of water (^{18}O , 2H) in the soil-plant-
600 atmosphere system, 2. Assessment under field conditions, *Chemical Geology*, 115, 317–



- 601 333, 1994.
- 602 Bowen, G. J.: The Online Isotopes in Precipitation Calculator, version 3.1., 2018.
- 603 Bowen, G. J. and Revenaugh, J.: Interpolating the isotopic composition of modern meteoric
604 precipitation, *Water Resources Research*, 39(10), 1–13, doi:10.1029/2003WR002086,
605 2003.
- 606 Brincat, D., Yamada, K., Ishiwatari, R., Uemura, H. and Naraoka, H.: Molecular-isotopic
607 stratigraphy of long-chain *n*-alkanes in Lake Baikal Holocene and glacial age sediments,
608 *Organic Geochemistry*, 31(4), 287–294, doi:10.1016/S0146-6380(99)00164-3, 2000.
- 609 Cappelen, J.: Danish Climatological Normals 1971-2000 - for selected stations., 2002.
- 610 Cernusak, L. A., Wong, S. C. and Farquhar, G. D.: Oxygen isotope composition of phloem sap
611 in relation to leaf water in *Ricinus communis*, *Functional Plant Biology*, 30(10), 1059–
612 1070, 2003.
- 613 Cernusak, L. A., Barbour, M. M., Arndt, S. K., Cheesman, A. W., English, N. B., Feild, T. S.,
614 Helliker, B. R., Holloway-Phillips, M. M., Holtum, J. A. M., Kahmen, A., Mcinerney, F.
615 A., Munksgaard, N. C., Simonin, K. A., Song, X., Stuart-Williams, H., West, J. B. and
616 Farquhar, G. D.: Stable isotopes in leaf water of terrestrial plants, *Plant Cell and
617 Environment*, 39(5), 1087–1102, doi:10.1111/pce.12703, 2016.
- 618 Coffinet, S., Huguet, A., Anquetil, C., Derenne, S., Pedentchouk, N., Bergonzini, L.,
619 Omuombo, C., Williamson, D., Jones, M., Majule, A. and Wagner, T.: Evaluation of
620 branched GDGTs and leaf wax *n*-alkane $\delta^2\text{H}$ as (paleo) environmental proxies in East
621 Africa, *Geochimica et Cosmochimica Acta*, 198, 182–193,
622 doi:10.1016/j.gca.2016.11.020, 2017.
- 623 Cormier, M.-A., Werner, R. A., Sauer, P. E., Gröcke, D. R., M.C., L., Wieloch, T., Schleucher,
624 J. and Kahmen, A.: ^2H fractionations during the biosynthesis of carbohydrates and lipids
625 imprint a metabolic signal on the $\delta^2\text{H}$ values of plant organic compounds, *New
626 Phytologist*, 218(2), 479–491, doi:10.1111/nph.15016, 2018.
- 627 Craig, H.: Isotopic Variations in Meteoric Waters, *Science*, 133, 1702–1703, 1961.
- 628 Dang, X., Yang, H., Naafs, B. D. A., Pancost, R. D. and Xie, S.: Evidence of moisture control
629 on the methylation of branched glycerol dialkyl glycerol tetraethers in semi-arid and arid
630 soils, *Geochimica et Cosmochimica Acta*, 189, 24–36, doi:10.1016/j.gca.2016.06.004,
631 2016.
- 632 Dansgaard, W.: Stable isotopes in precipitation, *Tellus*, 16(4), 436–468, doi:10.1111/j.2153-
633 3490.1964.tb00181.x, 1964.
- 634 Dawson, T. E., Mambelli, S., Plamboeck, A. H., Templer, P. H. and Tu, K. P.: Stable Isotopes
635 in Plant Ecology, *Annual Review of Ecology and Systematics*, 33(1), 507–559,
636 doi:10.1146/annurev.ecolsys.33.020602.095451, 2002.
- 637 Diefendorf, A. F. and Freimuth, E. J.: Extracting the most from terrestrial plant-derived *n*-alkyl
638 lipids and their carbon isotopes from the sedimentary record: A review, *Organic
639 Geochemistry*, 103(January), 1–21, doi:10.1016/j.orggeochem.2016.10.016, 2016.
- 640 Dirghangi, S. S., Pagani, M., Hren, M. T. and Tipple, B. J.: Distribution of glycerol dialkyl
641 glycerol tetraethers in soils from two environmental transects in the USA, *Organic
642 Geochemistry*, 59, 49–60, doi:10.1016/j.orggeochem.2013.03.009, 2013.



- 643 Dubbert, M., Cuntz, M., Piayda, A., Maguás, C. and Werner, C.: Partitioning evapotranspiration
644 - Testing the Craig and Gordon model with field measurements of oxygen isotope ratios
645 of evaporative fluxes, *Journal of Hydrology*, 496, 142–153,
646 doi:10.1016/j.jhydrol.2013.05.033, 2013.
- 647 DWD Climate Data Center: Historical annual precipitation observations for Germany. [online]
648 Available from: ftp://ftp-
649 cdc.dwd.de/pub/CDC/observations_germany/climate/hourly/precipitation/historical/
650 (Accessed 20 September 2018a), 2018.
- 651 DWD Climate Data Center: Historical hourly station observations of 2m air temperature and
652 humidity for Germany. [online] Available from: ftp://ftp-
653 cdc.dwd.de/pub/CDC/observations_germany/climate/hourly/air_temperature/historical/
654 (Accessed 19 September 2018b), 2018.
- 655 Eglinton, T. I. and Eglinton, G.: Molecular proxies for paleoclimatology, *Earth and Planetary
656 Science Letters*, 275(1), 1–16, 2008.
- 657 Feakins, S. J. and Sessions, A. L.: Controls on the D/H ratios of plant leaf waxes in an arid
658 ecosystem, *Geochimica et Cosmochimica Acta*, 74(7), 2128–2141,
659 doi:http://dx.doi.org/10.1016/j.gca.2010.01.016, 2010.
- 660 Feakins, S. J., Bentley, L. P., Salinas, N., Shenkin, A., Blonder, B., Goldsmith, G. R., Ponton,
661 C., Arvin, L. J., Wu, M. S., Peters, T., West, A. J., Martin, R. E., Enquist, B. J., Asner, G.
662 P. and Malhi, Y.: Plant leaf wax biomarkers capture gradients in hydrogen isotopes of
663 precipitation from the Andes and Amazon, *Geochimica et Cosmochimica Acta*, 182, 155–
664 172, doi:10.1016/j.gca.2016.03.018, 2016.
- 665 Freimuth, E. J., Diefendorf, A. F. and Lowell, T. V.: Hydrogen isotopes of *n*-alkanes and *n*-
666 alkanolic acids as tracers of precipitation in a temperate forest and implications for
667 paleorecords, *Geochimica et Cosmochimica Acta*, 206, 166–183,
668 doi:10.1016/j.gca.2017.02.027, 2017.
- 669 Frich, P., Rosenørn, S., Madsen, H. and Jensen, J. J.: Observed Precipitation in Denmark, 1961-
670 90., 1997.
- 671 Gamarra, B., Sachse, D. and Kahmen, A.: Effects of leaf water evaporative ²H-enrichment and
672 biosynthetic fractionation on leaf wax *n*-alkane δ²H values in C3 and C4 grasses, *Plant,
673 Cell and Environment*, 39, 2390–2403, doi:10.1111/pce.12789, 2016.
- 674 Gat, J. R.: Comments on the Stable Isotope Method in Regional Groundwater Investigations,
675 *Water Resources Research*, 7(4), 980–993, doi:10.1029/WR007i004p00980, 1971.
- 676 van Geldern, R., Baier, A., Subert, H. L., Kowol, S., Balk, L. and Barth, J. A. C.: (Table S1)
677 Stable isotope composition of precipitation sampled at Erlangen, Germany between 2010
678 and 2013 for station GeoZentrum located at Erlangen city center, in In supplement to: van
679 Geldern, R et al. (2014): Pleistocene paleo-groundwater as a pristine fresh water resource
680 in southern Germany – evidence from stable and radiogenic isotopes. *Science of the Total
681 Environment*, 496, 107–115, https://doi.org/10.1016/j., PANGAEA., 2014.
- 682 Guggenberger, G., Christensen, B. T. and Zech, W.: Land-use effects on the composition of
683 organic matter in particle-size separates of soil: I. Lignin and carbohydrate signature,
684 *European Journal of Soil Science*, 45(December), 449–458, 1994.
- 685 Helliker, B. R. and Ehleringer, J. R.: Grass blades as tree rings: environmentally induced
686 changes in the oxygen isotope ratio of cellulose along the length of grass blades, *New*



- 687 Phytologist, 155, 417–424, 2002.
- 688 Hepp, J., Rabus, M., Anhäuser, T., Bromm, T., Laforsch, C., Sirocko, F., Glaser, B. and Zech,
689 M.: A sugar biomarker proxy for assessing terrestrial versus aquatic sedimentary input,
690 Organic Geochemistry, 98, 98–104, doi:10.1016/j.orggeochem.2016.05.012, 2016.
- 691 Hepp, J., Wüthrich, L., Bromm, T., Bliedtner, M., Schäfer, I. K., Glaser, B., Rozanski, K.,
692 Sirocko, F., Zech, R. and Zech, M.: How dry was the Younger Dryas? Evidence from a
693 coupled $\delta^2\text{H}$ - $\delta^{18}\text{O}$ biomarker paleohygrometer, applied to the Lake Gemündener Maar
694 sediments, Western Eifel, Germany, Climate of the Past Discussions, (September), 1–44,
695 doi:10.5194/cp-2018-114, 2018a.
- 696 Hepp, J., Schäfer, I., Tuthorn, M., Glaser, B., Juchelka, D., Rozanski, K., Stichler, W., Zech,
697 R., Mayr, C. and Zech, M.: Validation of acoupled $\delta^2\text{H}_{n\text{-alkane}}$ - $\delta^{18}\text{O}_{\text{sugar}}$ paleohygrometer
698 approach based on a climate chamber experiment, submitted to GCA, 2018b.
- 699 Herrmann, A., Maloszewski, P. and Stichler, W.: Changes of ^{18}O contents of precipitation water
700 during seepage in the unsaturated zone, in Proceedings of International Symposium on
701 Groundwater Monitoring and Management, 23 - 28 March, p. 22, Institut of Water
702 Management Berlin (GDR) with support of UNESCO, Dresden., 1987.
- 703 Hopmans, E. C., Weijers, J. W. H., Schefuß, E., Herfort, L., Sinninghe Damsté, J. S. and
704 Schouten, S.: A novel proxy for terrestrial organic matter in sediments based on branched
705 and isoprenoid tetraether lipids, Earth and Planetary Science Letters, 224(1–2), 107–116,
706 doi:10.1016/j.epsl.2004.05.012, 2004.
- 707 Horita, J. and Wesolowski, D. J.: Liquid-vapor fractionation of oxygen and hydrogen isotopes
708 of water from the freezing to the critical temperature, Geochimica et Cosmochimica Acta,
709 58(16), 3425–3437, doi:http://dx.doi.org/10.1016/0016-7037(94)90096-5, 1994.
- 710 Hothorn, T., Bühlmann, P., Dudoit, S., Molinaro, A. and Van Der Laan, M. J.: Survival
711 ensembles, Biostatistics, 7(3), 355–373, doi:10.1093/biostatistics/kxj011, 2006.
- 712 Hou, J., D’Andrea, W. J. and Huang, Y.: Can sedimentary leaf waxes record D/H ratios of
713 continental precipitation? Field, model, and experimental assessments, Geochimica et
714 Cosmochimica Acta, 72, 3503–3517, doi:10.1016/j.gca.2008.04.030, 2008.
- 715 Huguet, A., Fosse, C., Metzger, P., Fritsch, E. and Derenne, S.: Occurrence and distribution of
716 extractable glycerol dialkyl glycerol tetraethers in podzols, Organic Geochemistry, 41(3),
717 291–301, doi:10.1016/j.orggeochem.2009.10.007, 2010a.
- 718 Huguet, A., Fosse, C., Laggoun-Défarge, F., Toussaint, M. L. and Derenne, S.: Occurrence and
719 distribution of glycerol dialkyl glycerol tetraethers in a French peat bog, Organic
720 Geochemistry, 41(6), 559–572, doi:10.1016/j.orggeochem.2010.02.015, 2010b.
- 721 IAEA/WMO: Global Network of Isotopes in Precipitation. The GNIP Database., 2015.
- 722 IAEA/WMO: Global Network of Isotopes in Precipitation. The GNIP Database., 2018.
- 723 Jacob, H. and Sonntag, C.: An 8-year record of the seasonal- variation of ^2H and ^{18}O in
724 atmospheric water vapor and precipitation at Heidelberg, Tellus, 43B(3), 291–300, 1991.
- 725 Kahmen, A., Schefuß, E. and Sachse, D.: Leaf water deuterium enrichment shapes leaf wax *n*-
726 alkane δD values of angiosperm plants I: Experimental evidence and mechanistic
727 insights, Geochimica et Cosmochimica Acta, 111, 39–49, doi:10.1016/j.gca.2012.09.004,
728 2013.



- 729 Knapp, D. R.: Handbook of Analytical Derivatization Reactions, John Wiley & Sons, New
730 York, Chichester, Brisbane, Toronto, Singapore., 1979.
- 731 Laursen, E. V., Thomsen, R. S. and Cappelen, J.: Observed Air Temperature, Humidity,
732 Pressure, Cloud Cover and Weather in Denmark - with Climatological Standard Normals,
733 1961-90., 1999.
- 734 Levene, H.: Robust Tests for Equality of Variances, in Contributions to Probability and
735 Statistics: Essays in Honor of Harold Hotelling, vol. 69, edited by I. Olkin, pp. 78–92,
736 Stanford University Press, Palo Alto, California., 1960.
- 737 Liu, W. and Yang, H.: Multiple controls for the variability of hydrogen isotopic compositions
738 in higher plant *n*-alkanes from modern ecosystems, *Global Change Biology*, 14(9), 2166–
739 2177, doi:10.1111/j.1365-2486.2008.01608.x, 2008.
- 740 Liu, Y., Wang, J., Liu, D., Li, Z., Zhang, G., Tao, Y., Xie, J., Pan, J. and Chen, F.: Straw
741 mulching reduces the harmful effects of extreme hydrological and temperature conditions
742 in citrus orchards, *PLoS ONE*, 9(1), 1–9, doi:10.1371/journal.pone.0087094, 2014.
- 743 McInerney, F. A., Helliker, B. R. and Freeman, K. H.: Hydrogen isotope ratios of leaf wax *n*-
744 alkanes in grasses are insensitive to transpiration, *Geochimica et Cosmochimica Acta*,
745 75(2), 541–554, doi:10.1016/j.gca.2010.10.022, 2011.
- 746 Merlivat, L.: Molecular diffusivities of H₂¹⁶O, HD¹⁶O, and H₂¹⁸O in gases, *The Journal of*
747 *Chemical Physics*, 69(6), 2864–2871, doi:http://dx.doi.org/10.1063/1.436884, 1978.
- 748 Mueller-Niggemann, C., Utami, S. R., Marxen, A., Mangelsdorf, K., Bauersachs, T. and
749 Schwark, L.: Distribution of tetraether lipids in agricultural soils - Differentiation
750 between paddy and upland management, *Biogeosciences*, 13(5), 1647–1666,
751 doi:10.5194/bg-13-1647-2016, 2016.
- 752 Oppermann, B. I., Michaelis, W., Blumenberg, M., Frerichs, J., Schulz, H. M., Schippers, A.,
753 Beaubien, S. E. and Krüger, M.: Soil microbial community changes as a result of long-
754 term exposure to a natural CO₂ vent, *Geochimica et Cosmochimica Acta*, 74(9), 2697–
755 2716, doi:10.1016/j.gca.2010.02.006, 2010.
- 756 Pedentchouk, N. and Zhou, Y.: Factors Controlling Carbon and Hydrogen Isotope Fractionation
757 During Biosynthesis of Lipids by Phototrophic Organisms, in *Hydrocarbons, Oils and*
758 *Lipids: Diversity, Origin, Chemistry and Fate. Handbook of Hydrocarbon and Lipid*
759 *Microbiology*, edited by H. Wilkes, pp. 1–24, Springer, Cham., 2018.
- 760 Peterse, F., van der Meer, J., Schouten, S., Weijers, J. W. H., Fierer, N., Jackson, R. B., Kim,
761 J. H. and Sinninghe Damsté, J. S.: Revised calibration of the MBT-CBT paleotemperature
762 proxy based on branched tetraether membrane lipids in surface soils, *Geochimica et*
763 *Cosmochimica Acta*, 96, 215–229, doi:10.1016/j.gca.2012.08.011, 2012.
- 764 Prietzel, J., Dechamps, N. and Spielvogel, S.: Analysis of non-cellulosic polysaccharides helps
765 to reveal the history of thick organic surface layers on calcareous Alpine soils, *Plant and*
766 *Soil*, 365(1–2), 93–114, doi:10.1007/s11104-012-1340-2, 2013.
- 767 R Core Team: R: A Language and Environment for Statistical Computing, [online] Available
768 from: <https://www.r-project.org/>, 2015.
- 769 Rach, O., Brauer, A., Wilkes, H. and Sachse, D.: Delayed hydrological response to Greenland
770 cooling at the onset of the Younger Dryas in western Europe, *Nature Geoscience*, 7(1),
771 109–112, doi:10.1038/ngeo2053, 2014.



- 772 Rao, Z., Zhu, Z., Jia, G., Henderson, A. C. G., Xue, Q. and Wang, S.: Compound specific δD
773 values of long chain *n*-alkanes derived from terrestrial higher plants are indicative of the
774 δD of meteoric waters: Evidence from surface soils in eastern China, *Organic*
775 *Geochemistry*, 40(8), 922–930, doi:<http://dx.doi.org/10.1016/j.orggeochem.2009.04.011>,
776 2009.
- 777 Romero-Viana, L., Kienel, U. and Sachse, D.: Lipid biomarker signatures in a hypersaline lake
778 on Isabel Island (Eastern Pacific) as a proxy for past rainfall anomaly (1942-2006AD),
779 *Palaeogeography, Palaeoclimatology, Palaeoecology*, 350–352, 49–61,
780 doi:10.1016/j.palaeo.2012.06.011, 2012.
- 781 Sachse, D., Radke, J. and Gleixner, G.: Hydrogen isotope ratios of recent lacustrine sedimentary
782 *n*-alkanes record modern climate variability, *Geochimica et Cosmochimica Acta*, 68(23),
783 4877–4889, doi:<http://dx.doi.org/10.1016/j.gca.2004.06.004>, 2004.
- 784 Sachse, D., Radke, J. and Gleixner, G.: δD values of individual *n*-alkanes from terrestrial plants
785 along a climatic gradient – Implications for the sedimentary biomarker record, *Organic*
786 *Geochemistry*, 37, 469–483, doi:10.1016/j.orggeochem.2005.12.003, 2006.
- 787 Sachse, D., Billault, I., Bowen, G. J., Chikaraishi, Y., Dawson, T. E., Feakins, S. J., Freeman,
788 K. H., Magill, C. R., McInerney, F. A., van der Meer, M. T. J., Polissar, P., Robins, R. J.,
789 Sachs, J. P., Schmidt, H.-L., Sessions, A. L., White, J. W. C. and West, J. B.: Molecular
790 Paleohydrology: Interpreting the Hydrogen-Isotopic Composition of Lipid Biomarkers
791 from Photosynthesizing Organisms, *Annual Reviews*, 40, 221–249,
792 doi:10.1146/annurev-earth-042711-105535, 2012.
- 793 Schäfer, I. K., Lanny, V., Franke, J., Eglinton, T. I., Zech, M., Vysloužilová, B. and Zech, R.:
794 Leaf waxes in litter and topsoils along a European transect, *SOIL*, 2, 551–564,
795 doi:10.5194/soil-2-551-2016, 2016.
- 796 Schlotter, D.: The spatio-temporal distribution of $\delta^{18}O$ and δ^2H of precipitation in Germany -
797 an evaluation of regionalization methods, Albert-Ludwigs-Universität Freiburg im
798 Breisgau. [online] Available from: [http://www.hydrology.uni-](http://www.hydrology.uni-freiburg.de/abschluss/Schlotter_D_2007_DA.pdf)
799 [freiburg.de/abschluss/Schlotter_D_2007_DA.pdf](http://www.hydrology.uni-freiburg.de/abschluss/Schlotter_D_2007_DA.pdf), 2007.
- 800 Schmidt, H.-L., Werner, R. A. and Roßmann, A.: ^{18}O Pattern and biosynthesis of natural plant
801 products, *Phytochemistry*, 58(1), 9–32, doi:[http://dx.doi.org/10.1016/S0031-](http://dx.doi.org/10.1016/S0031-9422(01)00017-6)
802 [9422\(01\)00017-6](http://dx.doi.org/10.1016/S0031-9422(01)00017-6), 2001.
- 803 Schmidt, H.-L., Werner, R. A. and Eisenreich, W.: Systematics of 2H patterns in natural
804 compounds and its importance for the elucidation of biosynthetic pathways,
805 *Phytochemistry Reviews*, 2(1–2), 61–85, doi:10.1023/B:PHYT.0000004185.92648.ae,
806 2003.
- 807 Schouten, S., Hopmans, E. C. and Sinninghe Damsté, J. S.: The organic geochemistry of
808 glycerol dialkyl glycerol tetraether lipids: A review, *Organic Geochemistry*, 54, 19–61,
809 doi:10.1016/j.orggeochem.2012.09.006, 2013.
- 810 Schreuder, L. T., Beets, C. J., Prins, M. A., Hatté, C. and Peterse, F.: Late Pleistocene climate
811 evolution in Southeastern Europe recorded by soil bacterial membrane lipids in Serbian
812 loess, *Palaeogeography, Palaeoclimatology, Palaeoecology*, 449, 141–148,
813 doi:10.1016/j.palaeo.2016.02.013, 2016.
- 814 Sessions, A. L., Burgoyne, T. W., Schimmelmann, A. and Hayes, J. M.: Fractionation of
815 hydrogen isotopes in lipid biosynthesis, *Organic Geochemistry*, 30, 1193–1200, 1999.



- 816 Shapiro, S. S. and Wilk, M. B.: An Analysis of Variance Test for Normality, *Biometrika*,
817 52(3/4), 591–611, doi:biomet/52.3-4.591, 1965.
- 818 Sternberg, L. S. L.: Comment on “Oxygen isotope ratios ($^{18}\text{O}/^{16}\text{O}$) of hemicellulose-derived
819 sugar biomarkers in plants, soils and sediments as paleoclimate proxy I: Insight from a
820 climate chamber experiment” by Zech et al. (2014), *Geochimica et Cosmochimica Acta*,
821 141, 677–679, doi:10.1016/j.gca.2014.04.051, 2014.
- 822 Strobl, C., Boulesteix, A. L., Zeileis, A. and Hothorn, T.: Bias in random forest variable
823 importance measures: Illustrations, sources and a solution, *BMC Bioinformatics*, 8,
824 doi:10.1186/1471-2105-8-25, 2007.
- 825 Strobl, C., Boulesteix, A. L., Kneib, T., Augustin, T. and Zeileis, A.: Conditional variable
826 importance for random forests, *BMC Bioinformatics*, 9, 1–11, doi:10.1186/1471-2105-9-
827 307, 2008.
- 828 Stumpp, C., Klaus, J. and Stichler, W.: Analysis of long-term stable isotopic composition in
829 German precipitation, *Journal of Hydrology*, 517, 351–361,
830 doi:10.1016/j.jhydrol.2014.05.034, 2014.
- 831 Sun, C. J., Zhang, C. L., Li, F. Y., Wang, H. Y. and Liu, W. G.: Distribution of branched
832 glycerol dialkyl glycerol tetraethers in soils on the Northeastern Qinghai-Tibetan Plateau
833 and possible production by nitrite-reducing bacteria, *Science China Earth Sciences*, 59(9),
834 1834–1846, doi:10.1007/s11430-015-0230-2, 2016.
- 835 Swedish Meteorological and Hydrological Institute: SMHI Open Data Meteorological
836 Observations., 2018.
- 837 Tipple, B. J., Berke, M. A., Hambach, B., Roden, J. S. and Ehleringer, J. R.: Predicting leaf
838 wax *n*-alkane $^2\text{H}/^1\text{H}$ ratios: Controlled water source and humidity experiments with
839 hydroponically grown trees confirm predictions of Craig-Gordon model, *Plant, Cell and*
840 *Environment*, 38(6), 1035–1047, doi:10.1111/pce.12457, 2015.
- 841 Tuthorn, M., Zech, M., Ruppenthal, M., Oelmann, Y., Kahmen, A., del Valle, H. F., Wilcke,
842 W. and Glaser, B.: Oxygen isotope ratios ($^{18}\text{O}/^{16}\text{O}$) of hemicellulose-derived sugar
843 biomarkers in plants, soils and sediments as paleoclimate proxy II: Insight from a climate
844 transect study, *Geochimica et Cosmochimica Acta*, 126, 624–634,
845 doi:http://dx.doi.org/10.1016/j.gca.2013.11.002, 2014.
- 846 Tuthorn, M., Zech, R., Ruppenthal, M., Oelmann, Y., Kahmen, A., del Valle, H. F., Eglinton,
847 T., Rozanski, K. and Zech, M.: Coupling $\delta^2\text{H}$ and $\delta^{18}\text{O}$ biomarker results yields
848 information on relative humidity and isotopic composition of precipitation - a climate
849 transect validation study, *Biogeosciences*, 12, 3913–3924, doi:10.5194/bg-12-3913-
850 2015, 2015.
- 851 Umweltbundesamt GmbH: Erhebung der Wassergüte in Österreich gemäß Hydrographiegesetz
852 i.d.F. des BGBl. Nr. 252/90 (gültig bis Dezember 2006) bzw.
853 Gewässerzustandsüberwachung in Österreich gemäß Wasserrechtsgesetz, BGBl. I Nr.
854 123/06, i.d.g.F.; BMLFUW, Sektion IV / Abteilung 3 N. [online] Available from:
855 https://wasser.umweltbundesamt.at/h2odb/fivestep/abfrageQdPublic.xhtml (Accessed 20
856 September 2018), 2018.
- 857 Walker, C. D. and Brunel, J.-P.: Examining Evapotranspiration in a Semi-Arid Region using
858 Stable Isotopes of Hydrogen and Oxygen, *Journal of Hydrology*, 118, 55–75, 1990.
- 859 Wang, C., Hren, M. T., Hoke, G. D., Liu-Zeng, J. and Garziona, C. N.: Soil *n*-alkane δD and



- 860 glycerol dialkyl glycerol tetraether (GDGT) distributions along an altitudinal transect
861 from southwest China: Evaluating organic molecular proxies for paleoclimate and
862 paleoelevation, *Organic Geochemistry*, 107, 21–32,
863 doi:10.1016/j.orggeochem.2017.01.006, 2017.
- 864 Wang, H., Liu, W., Zhang, C. L., Liu, Z. and He, Y.: Branched and isoprenoid tetraether (BIT)
865 index traces water content along two marsh-soil transects surrounding Lake Qinghai:
866 Implications for paleo-humidity variation, *Organic Geochemistry*, 59, 75–81,
867 doi:10.1016/j.orggeochem.2013.03.011, 2013.
- 868 Weijers, J. W. H., Schouten, S., Spaargaren, O. C. and Sinninghe Damsté, J. S.: Occurrence
869 and distribution of tetraether membrane lipids in soils: Implications for the use of the
870 TEX₈₆ proxy and the BIT index, *Organic Geochemistry*, 37(12), 1680–1693,
871 doi:10.1016/j.orggeochem.2006.07.018, 2006.
- 872 Weijers, J. W. H., Schouten, S., van den Donker, J. C., Hopmans, E. C. and Sinninghe Damsté,
873 J. S.: Environmental controls on bacterial tetraether membrane lipid distribution in soils,
874 *Geochimica et Cosmochimica Acta*, 71(3), 703–713, doi:10.1016/j.gca.2006.10.003,
875 2007.
- 876 Weijers, J. W. H., Wiesenberg, G. L. B., Bol, R., Hopmans, E. C. and Pancost, R. D.: Carbon
877 isotopic composition of branched tetraether membrane lipids in soils suggest a rapid
878 turnover and a heterotrophic life style of their source organism(s), *Biogeosciences*, 7(9),
879 2959–2973, doi:10.5194/bg-7-2959-2010, 2010.
- 880 Weijers, J. W. H., Steinmann, P., Hopmans, E. C., Schouten, S. and Sinninghe Damsté, J. S.:
881 Bacterial tetraether membrane lipids in peat and coal: Testing the MBT-CBT temperature
882 proxy for climate reconstruction, *Organic Geochemistry*, 42(5), 477–486,
883 doi:10.1016/j.orggeochem.2011.03.013, 2011.
- 884 Xie, S., Pancost, R. D., Chen, L., Evershed, R. P., Yang, H., Zhang, K., Huang, J. and Xu, Y.:
885 Microbial lipid records of highly alkaline deposits and enhanced aridity associated with
886 significant uplift of the Tibetan Plateau in the Late Miocene, *Geology*, 40(4), 291–294,
887 doi:10.1130/G32570.1, 2012.
- 888 Zech, M. and Glaser, B.: Compound-specific $\delta^{18}\text{O}$ analyses of neutral sugars in soils using gas
889 chromatography-pyrolysis-isotope ratio mass spectrometry: problems, possible solutions
890 and a first application, *Rapid Communications in Mass Spectrometry*, 23, 3522–3532,
891 doi:10.1002/rcm, 2009.
- 892 Zech, M., Rass, S., Buggle, B., Löscher, M. and Zöller, L.: Reconstruction of the late
893 Quaternary paleoenvironments of the Nussloch loess paleosol sequence, Germany, using
894 *n*-alkane biomarkers, *Quaternary Research*, 78(2), 226–235,
895 doi:10.1016/j.yqres.2012.05.006, 2012a.
- 896 Zech, M., Kreutzer, S., Goslar, T., Meszner, S., Krause, T., Faust, D. and Fuchs, M.: Technical
897 Note: *n*-Alkane lipid biomarkers in loess: post-sedimentary or syn-sedimentary?,
898 *Discussions, Biogeosciences*, 9, 9875–9896, doi:10.5194/bgd-9-9875-2012, 2012b.
- 899 Zech, M., Tuthorn, M., Detsch, F., Rozanski, K., Zech, R., Zöller, L., Zech, W. and Glaser, B.:
900 A 220 ka terrestrial $\delta^{18}\text{O}$ and deuterium excess biomarker record from an eolian
901 permafrost paleosol sequence, NE-Siberia, *Chemical Geology*,
902 doi:10.1016/j.chemgeo.2013.10.023, 2013.
- 903 Zech, M., Mayr, C., Tuthorn, M., Leiber-Sauheitl, K. and Glaser, B.: Reply to the comment of



- 904 Sternberg on “Zech et al. (2014) Oxygen isotope ratios ($^{18}\text{O}/^{16}\text{O}$) of hemicellulose-
905 derived sugar biomarkers in plants, soils and sediments as paleoclimate proxy I: Insight
906 from a climate chamber experiment. *GCA, Geochimica et Cosmochimica Acta*, 141(0),
907 680–682, doi:10.1016/j.gca.2014.04.051, 2014.
- 908 Zech, M., Zech, R., Rozanski, K., Gleixner, G. and Zech, W.: Do *n*-alkane biomarkers in
909 soils/sediments reflect the $\delta^2\text{H}$ isotopic composition of precipitation? A case study from
910 Mt . Kilimanjaro and implications for paleoaltimetry and paleoclimate research, *Isotopes*
911 in Environmental and Health Studies, 51(4), 508–524,
912 doi:10.1080/10256016.2015.1058790, 2015.
- 913 Zech, R., Gao, L., Tarozo, R. and Huang, Y.: Branched glycerol dialkyl glycerol tetraethers in
914 Pleistocene loess-paleosol sequences: Three case studies, *Organic Geochemistry*, 53, 38–
915 44, doi:10.1016/j.orggeochem.2012.09.005, 2012c.